CFD ANALYSIS OF A POOL FIRE IN AN OFFSHORE PLATFORM

Author: Aleksandra Danuta Mielcarek

Supervisors: Professor Aldina Maria da Cruz Santiago
Professor Filippo Gentili

University: University of Coimbra

European Commission
ERASMUS MUNDUS

University: University of Coimbra

Date: 05.02.2016

ACKNOWLEDGEMENT

I acknowledge, with gratitude, my debt of thanks to Professor Aldina Santiago and Filippo Gentili for great supervision, their opinion and reviewing my report.

Deserving special mention is Professor Adam Glema from Poznań University of Technology for motivating me and supporting from the very beginning of my SUSCOS studies.

I would like to express my gratitude to Michał Malendowski for his guidance and the time he spent to help me, especially with the problems that I was facing with FDS software.

Special thanks to Wojciech Szymkuć, Karolina and Wojtek, who helped me to run FDS models.

I am very grateful for my best friends from my stay abroad, especially my flatmates from Napoli and Coimbra.

My love goes to my family who never stopped supporting me, in particular during the toughest times.

And thanks to the God for the best guidance.

ABSTRACT

One of the most important aspects in the design of the offshore platforms is related to natural hazards and catastrophic events such as wind storm, wave, earthquake, explosion and fire. Computational Fluid Dynamics (CFD) modelling, which enables to examine complex structures affected by selected fire scenarios, has become one of the most common tools in the fire engineering, also in case of offshore platforms. Fires on offshore platforms are large, in the open air, hydrocarbon usually with a very rapid heat release. Unfortunately, this type of field models results in problems with their validation since there is a huge gap in analytical methods that could be used for this purpose. For the fire risk assessment, numerous experiments were performed in order to introduce analytical methods. However, these analytical approaches are valid only for particular conditions. The limitations are associated with the experimental environment on which they are based.

Regarding the analytical models, EN 1991-1-2 presents a simplified calculation model developed by Heskestad to assess localised fires in case of fire in open air. However, this method shows some limitations: only the temperature in the plume is calculated and, if the wind effect is considered, the method is no longer applicable. Moreover, it is questionable to use Heskestad approach for large pool fires, since the experiments on which the method is based were conducted for smaller scale fires. There are also some analytical models for determining the radiative heat flux: Shokri and Beyler model, Mudan and Croce model and Modified Solid Flame model. However, they also show some limitations, especially due to the shape of the fire area by assuming that the fire flame is cylindrical. Due to the complex conditions, validation and accuracy of offshore fires and their field models is still uncertain.

In this thesis, a numerical simulation of a full-scale hydrocarbon pool fire is performed in FDS software. The study case corresponds to a “fictitious” fixed offshore platform which dimensions are based on the typical offshore platform. It is defined as an open structure composed by three main decks and two intermediate decks, steel frames, compartments and helideck. Fire scenarios assume an accidental crude oil leakage, which spreads and results in a localised pool fire. Modelled scenarios vary due to the localisation of the fire, its size, the total heat release rate and wind conditions. The results from the FDS model are compared with the available analytical methods.

It is observed that smaller grid sizes in FDS models give better prediction of the temperature in the plume along its symmetrical vertical axis if compared to the temperatures assessed by the expression given in EN 1991-1-2 for localised fires.

The outcomes for the radiative heat fluxes from FDS models are within the values predicted by the analytical models. However, the deviation in the results from all considered methods was observed which arises from different assumptions that the analytical correlation are based on as well as the input parameters used for the numerical modelling.

TABLE OF CONTENTS

INDEX OF FIGURES

INDEX OF TABLES

NOTATIONS

Latin upper case letters

A_f	horizontal burning area of the fire source
C	non-dimensional constant
D	diameter of a burning area
D^*	characteristic fire diameter
E	total emissive power of flame
E_{max}	equivalent black body emissive power (=140 kW/m^2)
E_s	emissive power of smoke (=20 kW/m^2)
$F_{1\to2}$	geometric view factor, configuration factor, shape factor
$F_{1\to2,H}$	configuration factor for horizontal target orientation
$F_{1\to2,\max}$	maximum configuration factor
$F_{1\to2,V}$	configuration factor for vertical target orientation
H	distance between fire source and ceiling – in case of localised fires
H	height of the luminous flame region – in case of radiation models
H_f	flame height
L	length of a fire base
L_f	flame length
P	perimeter of the fire
$\dot{Q}$	total heat release rate
Q_c	convective part of the rate of heat release Q
Q_D^*	heat release coefficient related to the diameter D of the local fire
Q_H^*	heat release coefficient related to the height H of the compartment
R	distance from the centre of the fire to the target
S	distance from the centre of the radiating plane to the target
S'	distance from the centreline of the radiating surface to the target
T_f	flame temperature
T_g	focal gas temperature
T_G	gauge temperature
T_w	surface temperature
T_∞	ambient air temperature (=293 K)
W	width of a fire base

Latin lower case letters

c_p	air thermal capacity (=1.0 kJ/kgK)
g	gravitational acceleration (=9.81 m/s^2)

$\dot{h}$	heat flux to unit surface area
hr	hour
$\dot{h}_{net}$	net heat flux to unit surface area
$\dot{h}_{net,c}$	net heat flux to unit surface area due to convection
$\dot{h}_{net,r}$	net heat flux to unit surface area due to radiation
k	extinction coefficient (=0.05 m^{-1})
$\dot{m}''$	pool mass loss rate
$\dot{m}''_{still}$	pool mass loss rate in case of no-wind
$\dot{m}''_{windy}$	pool mass loss rate in case of wind conditions
$\dot{m}''_{\infty}$	infinite-diameter pool mass loss rate
$\dot{q}''$	thermal radiation flux
$\dot{q}''_{conv}$	convective heat flux
$\dot{q}_f''$	heat release rate per unit area
$\dot{q}''_{gauge}$	gauge heat flux
$\dot{q}''_{inc}$	incident heat flux
$\dot{q}''_{net}$	net heat flux
$\dot{q}''_{rad}$	radiative heat flux
$\dot{q}''_{rad,in}$	radiative heat flux incoming (absorbed)
$\dot{q}''_{rad,out}$	radiative heat flux outgoing (reflected)
$\dot{q}''_{radiometer}$	radiometer heat flux
s	second
s	extinction coefficient (=0.12 m^{-1})
t	time
u^*	non-dimensional wind velocity
u_w	wind velocity
v	wind velocity
y	coefficient parameter
z	height
z'	vertical position of the virtual heat source
z_0	virtual origin of the height z

Greek upper case letters

Δh_c	lower heat of combustion
θ_g	gas temperature
θ_m	temperature of the member surface
$\theta_{(z)}$	gas temperature at height z
Φ	configuration factor

Greek lower case letters

α_c	coefficient of heat transfer by convection
β	mean beam length corrector

δx	nominal size
ε_f	emissivity of flames, of fire
ε_m	surface emissivity of the member
ρ_a	ambient air density
ρ_∞	air density (=1.2 kg/m^3)
σ	Stephan-Boltzman constant (=5,67· 10^{-8} W/m^{2}K^4)
χ_r	fraction of thermal radiation

ABBREVIATIONS

ASD	Acceptable Separation Distance
CFD	Computational Fluid Dynamics
CPU	Central Processing Unit
DNS	Direct Numerical Simulation
EC	Eurocode
EN	European Norm
FDS	Fire Dynamics Simulator
FRP	Fibre-reinforced Plastic
GUIs	Graphical User Interfaces
HRR	Heat Release Rate
HRRPUA	Heat Release Rate Per Unit Area
HRRPUV	Heat Release Rate Per Unit Volume
HUD	Housing and Urban Development
ISO	International Standard Organization
LES	Large Eddy Simulation
MPI	Message Passing Interface
NIST	National Institute of Standards and Technology
OpenMP	Open Multi-Processing
RAM	Random Access Memory
SUSCOS	Sustainable Constructions under Natural Hazards and Catastrophic Events

1. INTRODUCTION

Offshore platforms are marine structures which are widely used in oil and gas exploitation. Their design has to satisfy rigorous requirements taking into account often complex geotechnical and environmental conditions. There are different types of offshore platforms. However, the super-structures (topside) are common features associated with the various types of offshore platforms. Topside consists of a number of modules that host different equipment (gas turbine, pumps, gas flare stack, living quarters with hotel). Most of these modules are highly congested with the presence of obstacles in the form of pipelines, cables and other equipment necessary for process operations.

Additionally, offshore platforms work with highly combustible materials as oil and gas. The level of risk in such conditions is very high [1]. Explosions followed by hydrocarbon fires are the most frequently reported incidents on offshore platforms. These fires predominantly occur in well ventilated open decks, involving burning oils and gaseous components with an enormous release of energy. There is an endless number of fire scenarios that could possibly happen on the offshore platform with unknown effect on the whole structure. Thus, the fire hazard and risk assessment on the offshore platforms is still a challenge for the fire engineers.

In offshore platforms, depending on the location within the platform where the fire may be likely to occur, two major categories of fires are identified: cellulosic fires and hydrocarbon fires. Cellulosic fires, as indicated by the name, are fires with a fuel source mostly of cellulose (wood, paper, furniture, etc.). They are characterised by relatively slow growing phase and in case of offshore platforms they occur mainly in the accommodation areas. Conversely, hydrocarbon fires have a very rapid heat increase. Hydrocarbon fires are fuelled by oil and gas and occur predominantly outside the compartments, in the open area, what leads to fuel conducted fires. There are distinguished two types of hydrocarbon fires:

- a pool fire - involves burning liquid and is characterised by emitting turbulent flames;
- a jet fire – refers to the combustion of gaseous hydrocarbon and emits vigorous flame.

Since the fire occurs on the offshore platform, the structure is subjected to both convection and radiation. The latter one corresponds to hydrocarbon content and soot production. The convection is related to fluid velocity and is derived from hot gases. It is known that for large pool fires the burning is dominated by the radiative heat transfer from the flame surface and it is the main reason for the injury of a personnel and damage of the structure.

The pool hydrocarbon fires affecting the offshore platform are modelled in FDS software. The main aim of this thesis is to verify these numerical models with available analytical methods. First, two localised fires are modelled and investigated with a simplified calculation models developed by Heskestad and Hasemi which are presented in EN 1991-1-2. Two other scenarios refer to much bigger pool fires so the approach from Eurocode cannot be used anymore. They correspond to more realistic situations of the fire on the offshore platform. In case of large, open hydrocarbon fires the thermal radiation is the major mechanism for injury or damage. From this reason this aspect is studied and verified by analytical radiation model.

2. FIRE ANALYSIS

2.1 Thermal analysis according to EN 1991-1-2

2.1.1 Overview to design methods

The requirements of fire safety are clearly defined, taking into consideration the risk posed by fire and the level of acceptable risk. There are two approaches given by Eurocode to characterise the structural fire design, very general:

- the prescriptive based method which is simpler and refers to fire safety based on elements;

- the performance based method which is more complex but at the same time more accurate and concerns fire safety of a structure.

In general, it is required in the design and analysis of structures that their elements have enough load bearing resistance under the fire condition. Nevertheless, in case of performance based approach a wide range of expertness and qualification are required to numerically model structures that behave as close as possible to the real structural behaviour.

2.1.2 Prescriptive based method

Prescriptive based method, also called “deem to satisfy” method, says what solutions should be undertaken to provide that a design satisfies the regulations [2]. It defines limits that cannot be exceeded. The current prescriptive rules are based on traditional design techniques, experience and results and observations from standard fire resistance tests.

Standard fire tests rely on subjecting a structural element to a high temperature. Specimens are placed in gas burners for the desired duration. The test follows the standard temperature-time curve, without any cooling phase. The results are expressed as the time in minutes that the member is capable to withstand before a specified failure criterion is reached [3]. These elements are classified into fire resistance categories as follows: R15, R30, R60, R120 and R240. This specified period of time may be given in the national legislation or obtained from annex F following the specifications of the national annex. In Portugal the applied legislation is: 1532/2008 [4] and DL220/2008 [5].

The standard time-temperature curve (ISO 834) has over 100 year history. First attempts dates from 1890's and were requested by insurance companies. First curve was published in 1917 in US. The standard fire was obtained by conducting a lot of tests representing the worst case fires in enclosures. The standard fire was created by collating those various tests into one idealised curve. It was drawn before scientific understanding of fire dynamics. The standard fire ignores the effect of real fires. It has relatively slow growth period, never reduces in temperature due to the fire decay and is independent of building characteristics such as geometry, ventilation and fuel load [6]. Additionally to the ISO 834 curve from 1985 (standard temperature-time curve, cellulosic curve), Eurocode presents two other nominal curves – external fire curve and hydrocarbon curve (Figure 1). Moreover, PD 7974-1 provides alternative fire curve for large pool hydrocarbon fire [7]:

$$\theta_g = 1100(1 - 0{,}325e^{-0{,}167t} - 0{,}204e^{-1{,}417t} - 0{,}471e^{-15{,}833t}) + 20 \qquad (2.1)$$

Prescriptive approach is relatively easy to understand and apply, no complex calculations are required. In addition, experience has shown that this method ensures a minimum level of fire safety of the structures. It is fairly precise in terms of the materials used, shape and size of structural elements and thickness of fire protections. On the other hand, another disadvantage is that all elements are treated independently. The interaction can bring a possible beneficial effect when alternative load-path mechanisms are created. On the contrary, thermal expansion of members can be restrained what results in large compressive forces being induced into elements, usually vertical, causing instability of members. Prescriptive based method does not account for actual structural behaviour, levels of safety and robustness are unknown [8].

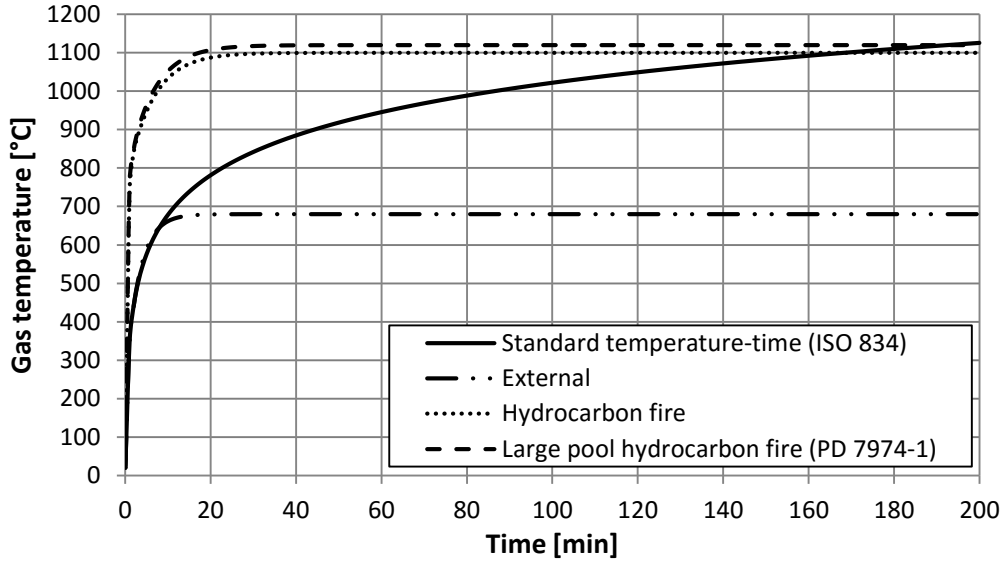

Figure 1. Nominal temperature-time curves

2.1.3 Performance based method

For some aspects the prescriptive based method cannot be used due to its restrictive nature. In this case the performance based method is presented in codes. This approach refers to thermal actions based on physical and chemical parameters. In general, the performance based approach incorporates three fundamental components, namely: the likely fire behaviour, the temperature evolution within the structure and its response due to the fire. The complexity of the design is related to the assumptions which are made and the selection of the methods to predict each of the components [3].

For fire modelling, performance based method requires selection of simple or advanced fire development models. Both models are called natural fire models. The input parameters for each of these models are quite different starting from little input parameters for simple models and ending with detailed input data for advanced models.

Simplified fire models

Simplified fire models include compartment fires and localised fires. In case of the first mentioned, it is assumed a uniform temperature distribution within the compartment as a function of time. The gas temperature is calculated using parametric temperature-time curve. Parametric curves, contrary nominal curves, include the cooling phase due to the fire decay. Moreover, the input parameters are more detailed. Determination of the gas temperature requires specification of fire load, ventilation conditions, thermal properties of boundary and compartment size.

Parametric temperature-time curve is based on a Swedish guidance document produced in 1976 [9]. It was a relatively vital breakthrough in structural fire analysis. The guide incorporated the current knowledge and understanding of compartment fire engineering verified by small-scale tests. The Swedish document presented a series of temperature-time curves for a broad scope of crucial parameters. All of the diagrams were collapsed into a simplified mathematical form named temperature-time curve [6].

Parametric fires give more realistic estimation of the fire severity compared with standard fires. Even though, they are not applicable for many modern buildings which are more complex in terms of structural solutions, new materials and mixed building technology. Innovative structures often do not satisfy limitations imposed by Eurocode to use nominal or parametric curves. These restrictions are closely related to the size and geometry of the experimental enclosures, usually small cubic compartments, which were used to perform tests and the obtained data is a methods basis. Eurocode says that they are valid only for fire compartments up to 500 m^2 of floor area and up to 4 m in height. In addition, the roof should not have openings.

Each case beyond the recommended range of applicability needs to be cautiously considered [6].

Another simplified fire model is localised fire. Compared with standard and parametric fires, localised fires are characterised by low probability of flashover. Due to this phenomenon, only pre-flashover fires are considered and the gas temperature is not anymore assumed to be uniform within the fire compartment. The temperature of the fire flame and plume and the surrounding gas have to be specified individually [3]. The simplified fire models are not enough to predict the smoke migration and fire spread. To obtain more detailed analysis, the advanced fire models are needed.

Advanced fire models

The advanced fire models use computer programs to simulate the heat and mass transfer related to a compartment fire. Advances in computers and numerical methods lead to more accurate prediction of the gas temperatures in a compartment. These models can also estimate the smoke flow and fire spread. Eurocode presents three advanced fire models, as follows: one-zone models, two-zone models and Computational Fluid Dynamic models (CFD).

One-zone models should be applied only for fully developed, post-flashover fires. Gas temperature, gas density, internal energy and pressure of the gas are assumed to be uniform in the compartment. The basics of one-zone models solve the governing differential equations for the conservation of mass and energy in the compartment [10].

Two-zone models are based on the assumption of accumulation of combustion products in a layer beneath the ceiling, with a horizontal interface. Different zones are defined: the upper layer, the lower layer, the fire and its plume, the external gas and walls. The upper layer is assumed to have time dependent thickness and time dependent uniform temperature, as well as the lower layer is assumed to have time dependent uniform but lower temperature. The fundamentals of two-zone models are also solving the governing differential equations for the conservation of mass and energy but separately for each zone and the exchange of mass and energy between two zones is calculated [10].

One-zone and two-zone models are used sequentially – first two-zone model is applied and after flashover the one-zone model is used. Both zone models require very detailed input data concerning fire load, ventilation conditions, thermal properties of boundary, compartment size, heat and mass balance system. More detailed input parameters results in better outcome.

The Computational Fluid Dynamics fire models, known as CFD models, are the most advanced but at this same time the most accurate available fire modelling techniques. Computational

domain is discretized into finite elements and fluid dynamics are employed to each element and numerically solve the conservation equations of mass, species, momentum and energy. These principal equations of the fluid flow are Navier-Stokes equations adequate for thermally driven flow and low-speed. They allow evaluate the temperature distribution over the time in the whole compartment. This thesis is mainly focused on CFD models. More detailed information about this approach is given in section 2.2.

2.2 CFD analysis

2.2.1 State of art on CFD studies

CFD based methods are widely applied during the design of offshore structures. They are used to examine fluid flow as well as heat transfer behaviour. In the first case, CFD models provide information including wave impact, air gap under offshore platform and influence of the wind. The second area of using CFD methods pertains to heat transfer. It is of high importance to investigate the behaviour of offshore fires and the structure exposed to high temperatures so that CFD models have become an inherent tool in structural and fire safety design of offshore platforms.

There are several previous research studies referring generally to fire modelling. Mostly they are focused on comparing sophisticated CFD models with available analytical methods or experimental data. Some of them are stated below but only those which use Fire Dynamic Simulator (FDS).

First it has to be highlighted that a lot of experimental data were used to validate FDS software. These data can be found in the FDS Validation Guide [11]. Nevertheless, to make the software more accurate and reliable tool, there are still ongoing researches. For example, Wang et al. [12] present additional study on a fire-induced flow which is a follow-up to previous study used for the validation of the FDS software. This work is based on so called “Steckler Compartment Experiments” from 1979 [13]. The study provides a vital improvements to the prediction of mass flow rates for the considered cases.

Widely modelled scenarios in FDS refer to localised fires. Zhang and Li [14] examined a thermal action from localised fires in large enclosures. Gas temperature and heat transfer from the fire to a vertical column was the case of the study but emphasis was put also on the effect of input parameters. In 2015 the same authors compared simple fire models with sophisticated fire models to predict the performance of a square hollow steel column exposed to a localised fire. The steel temperature predictions for both methods ensured that the classic fire plume theory yields conservative results, what means that it can be used in structural fire engineering [15].

CFD based methods have started to be used for travelling fires since the last decade. One of the fires study in this area was done by Rein et al. [16] where CFD method was applied to complex high-rise building and the comprehensive analysis of the fire environment was done. Sandström et al. [17] by studying the concept of travelling fires in FDS show that CFD model gives the results which are within the reasonable agreement with two-zone models. However, they state that this technique needs more study for more complex geometries. Stern-Gottfried and Rein present the literature review of the research concerning the travelling fire [18] and the design methodology for travelling fires [19].

One of the most important aspects while modelling in FDS refers to the sensitivity of the results due to grid resolution. This study was done by Petterson [20] by comparing the results with two separate sets of experiments. This study proved the importance of selecting a proper grid size to obtain reliable results. The same conclusion is reached by Kelsey et al. [21] which additionally examine the effect of the input variables such as the burn rate, fire diameter, radiative fraction and turbulence model, on the large scale LNG fire plume.

2.2.2 Overview on FDS software

FDS is Computational Fluid Dynamics software developed by the National Institute of Standards and Technology (NIST). Due to better computers capacity and more complex geometry of many modern buildings, it has started to be more popular since last decade. Commercial applications of FDS employ a large-eddy simulation (LES) turbulence model which is much less demanding in terms of grid resolution if compared to direct numerical simulation (DNS). LES assumes that combustion is controlled by turbulent mixing of combustion gases with the atmosphere around [22]. The domain of the FDS field model is divided into 3D grid elements which size is controlled by users.

FDS program runs from a command prompt line, not a graphical interface. It reads input parameters from a text file. However, there are FDS Graphical User Interfaces (GUIs) delivered by the third party providers to help in quick creating and managing the details of complicated fire models. Unlike to FDS software, they are not free but they are also not essential. Following GUIs were developed to make the modelling more convenient: PyroSim (Thunderhead Engineering), ASPIRE Smoke Detection Simulation (Xtralis), BlenderFDS (Emanuele Gissi), CYPE-Building Services (CYPE), Project Scorch (Autodesk). There is no indication that they are best suited for the intended purpose and NIST has not constituted endorsement for them. Smokeview is an associated program, also developed by NIST, which enables to read the output files and to see the animations.

FDS models provide a detailed understanding of the fire phenomena that cannot be obtained from any of the analytical method. The emphasis is put on the heat transport and smoke

migration from fires. FDS is highly valued program by fire safety engineers since it provides information about the smoke migration, concentration of the toxic combustion products (for example carbon monoxide concentration) and the visibility. All these parameters are needed in the escape routes design. Moreover, many modern buildings are characterised by complex geometry and large open spaces what impose the necessity to use CFD software.

Development in computer capabilities had a huge contribution to the increasing use of FDS software and what is important it is used not only by the scientific community nowadays. The robustness and accuracy of FDS requires a multi-core processor, satisfying amount of RAM and a large hard drive to store the output files. Starting with 6.1.0 FDS version, Open MPI programming interface is employed by default. Contrary to the previous versions where only a single core could be used for a given calculation, Open MPI enables most Windows-based personal computers to exploit multiple cores. What is more, dividing the computational domain into multiple meshes, make it possible to use MPI (Message-Passing Interface). In this case a single FDS job can be run on multiple computers [22]. As can be seen, the capabilities of FDS are still improved to make it not only more accurate software but also user-friendly.

The fast CPU and required amount of RAM are still a challenge even for good computers currently available on the market. The CPU speed delimits the time needed to run the analysis. The amount of RAM decides on the number of cells which can be held in a virtual memory. Moreover, FDS results are very dependent upon the grid resolution what has to be kept in mind of fire engineers.

2.2.3 Calibration of the numerical model

The objective of the presented calibration study is to gain confidence in the use of FDS software. For the sake of validation a numerical analysis is done based on the previous studies. The FDS model of a compartment with wooden fuels is created and the results from travelling fire are compared with those published in [23]. The model which is used reflects a previous full-scale travelling fire test.

The study is done to show that real fires in large compartments do not grow uniformly over an entire floor area. Fires tend to start at one point and then move across the enclosure as flames spread. The assumption that the temperature is evenly distributed within the compartment coincides with the small enclosures. The behaviour of real fires is different but traditional methods deem to be conservative and therefore they were appropriate to use them for the structural fire design [23].

In the examined model the compartment is 12 m long, 9 m in wide and 4 m high. The source of the fire was created by the wooden cribs of 0.05 x 0.05 x 1.0 m. The cribs formed 8 x 3 piles

closely spaced. Each pile consisted of 41 cribs (Figure 2). Ignition temperature and heat release rate per unit area (HRRPUA) of the wood were found by the calorimeter tests.

In the published model the computational domain was 13 m by 10.8 m by 4.2 m (slightly bigger than the dimensions of the compartment). The mesh around the wooden piles and the steel beam is 0.05 m by 0.05 m by 0.05 m and in the remaining part 0.1 m by 0.1 m by 0.1 m. In total the computational domain was composed of 24 parts what enabled to run the FDS job parallel on the cluster. This grid size resulted in a long run time. In order to decrease CPU time in the validation model, the mesh around wooden piles is still 0.05 m but in the remaining part it is 0.2 m by 0.2 m by 0.2 m.

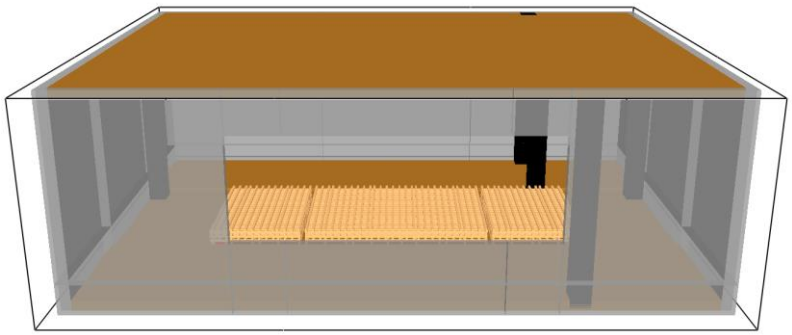

Figure 2. FDS model - outside view [23]

The walls of the compartment were made up of two materials - outside mineral wool (0.12m thick) and inside concrete (0.20 m thick). There was the opening located on the south wall – 6.0m wide and 2.0 m high. The CFT columns were made up also of two materials – steel (0.01 m thick) and concrete (0.15 m thick). Properties of the materials used in the model are shown in Table 1.

Table 1. Properties of the materials used in the FDS model [23]

	Concrete	**Steel**	**Mineral wool**	**Softwood**
Emissivity [-]	0.85	0.80	0.85	0.90
Density [kg/m^3]	2300	7850	40	400
Specific heat capacity [kJ/kgK]	1.05	0.60	0.84	1.3
Heat conductivity [W/mK]	1.40	45	0.04	0.2
Heat of combustion [kJ/kg]	-	-	-	18 000

In the calibrated model, simple pyrolysis is used by defining a gas burner located on the left side of the piles. It is activated for the first 300 s to enable the ignition of the wooden piles at the temperature of 245 °C with HRRPUA equal to 200.0 kW/m^2.

Figure 3 shows that the results from the validation simulation are comparable with the published. The variations of the HRR are very close. However, there is a difference around 3.7 MW in the value of the maximum heat release rate. In the calibration, in order to decrease the run time, bigger grid size was used what resulted in these variations.

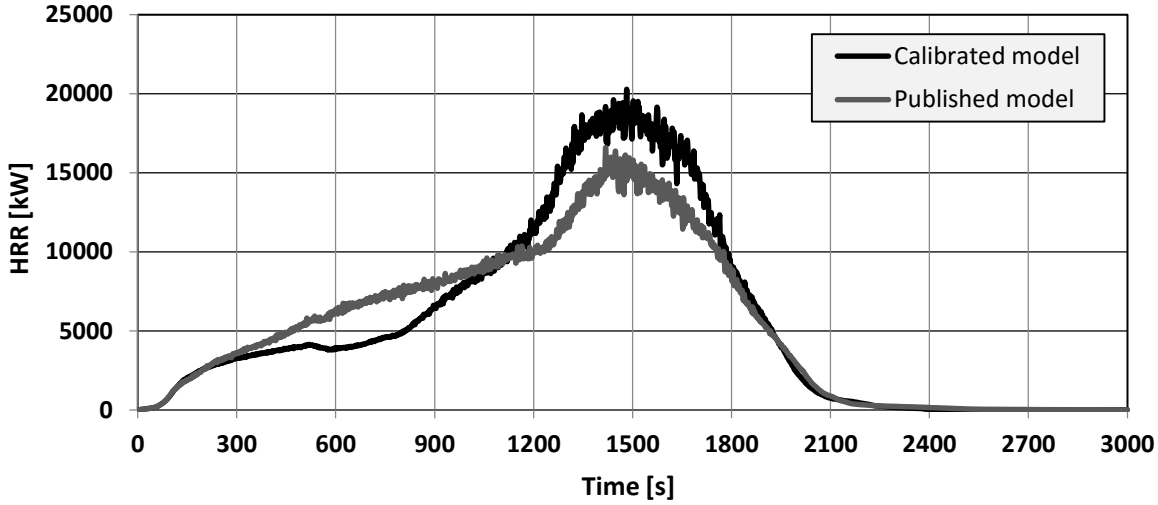

Figure 3. Comparison of HRR for published and calibrated data

2.3 Overview of localised fires according to EN 1991-1-2

Localised fire approach uses Heskestad's and Hasemi's methods. The flame length is calculated from Heskestad's equation (Figure 4):

$$L_f = -1.02D + 0.0148\dot{Q}^{2/5} \tag{2.2}$$

For relatively low fires, when the height of the flame is smaller than the distance between the fire source and the ceiling (H), the calculation of the temperature in the plume along the vertical flame axis is based on Heskestad's model. This approach is valid for open air fires as well:

$$\theta_{(z)} = 20 + 0.25{Q_c}^{2/3}(z - z_0)^{-5/3} \quad \leq \quad 900\ [°C] \tag{2.3}$$

Where:

$$z_0 = -1.02D + 0.00524Q^{2/5} \tag{2.4}$$

and

Q_c - the convective part of the heat release rate [W], with Q_c=0.8 Q by default;

z - the height along the flame axis [m].

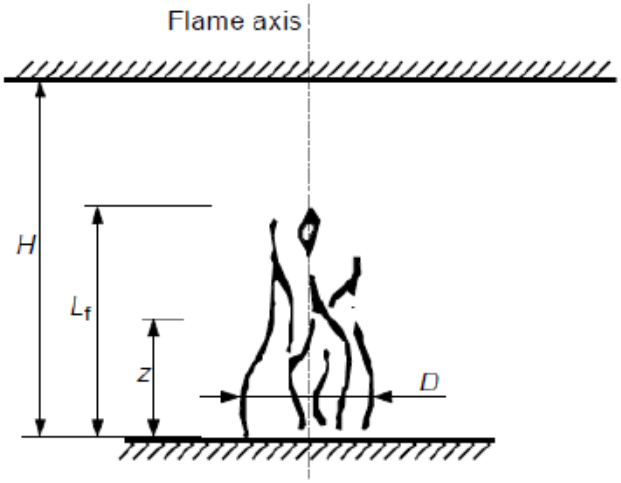

Figure 4. Denotation for small localised fires [10]

On the fire exposed surfaces, the net heat flux is determined by considering heat transfer by convection and radiation:

$$\dot{h}_{net} = \dot{h}_{net,c} + \dot{h}_{net,r} \tag{2.5}$$

The net convective heat flux component is determined by:

$$\dot{h}_{net,c} = \alpha_c . (\theta_{(z)} - \theta_m) \tag{2.6}$$

Where α_c is the coefficient of heat transfer by convection and θ_m is the surface temperature of the member.

The net radiative heat

$$\dot{h}_{net,r} = \Phi \, . \varepsilon_m . \varepsilon_f . \sigma . [(\theta_{(z)} + 273)^4 - (\theta_m + 273)^4] \tag{2.7}$$

Where:

- Φ - the configuration factor (=1.0);
- ε_m - the surface emissivity of the member (=0.8)
- ε_f - the emissivity of the fire (=1.0);
- σ - the Stephan Boltzmann constant (= $5.67 \cdot 10^{-8}$ W/m^{2}K^4).

When a localised fire is large enough, the flame impacts the ceiling of the compartment – it turns and travels horizontally underneath the ceiling. Eurocode [10] provides some design formulas based on Hasemi's fire plume model. It allows find the heat flux received by the

surface area at the ceiling level but it does not provide procedure for calculating the temperature in the plume.

The horizontal flame length is given by the following expression:

$$L_h = (2.9H(Q_H^*)^{0,33}) - H \tag{2.8}$$

With non-dimensional heat release rate obtained from:

$$Q_H^* = \frac{\dot{Q}}{(1.11 \cdot 10^6 \cdot H^{2,5})} \tag{2.9}$$

The heat flux $\dot{h}$ received by the fire exposed unit surface area at the ceiling level at the distance r from the flame axis is given by:

$$\dot{h} = \begin{cases} 100\,000, & \text{if } y \leq 0.30 \\ 136\,300\ to\ 121\,000\ y, & \text{if } 0.30 < y < 1.0 \\ 15\,000\ y^{-3,7}, & \text{if } y \geq 1.0 \end{cases} \tag{2.10}$$

Where:

$$y = \frac{r + H + z'}{L_h + H + z'} \tag{2.11}$$

and

- r - the horizontal distance from the vertical flame axis to the point along the ceiling where the thermal flux is calculated [m];
- z' - the vertical position of the virtual heat source as given by Equation 2.12 [m].

The vertical position of the virtual heat source:

$$z' = \begin{cases} 2.4D(Q_D^{*2/5} - Q_D^{*2/3}), & when\ Q^*{}_D < 1.0 \\ 2.4D(1.0 - Q_D^{*2/5}), & when\ Q^*{}_D \geq 1.0 \end{cases} \tag{2.12}$$

With:

$$Q^*{}_D = \frac{\dot{Q}}{(1.11 \cdot 10^6 \cdot D^{2,5})} \tag{2.13}$$

The net heat flux received by the fire exposed unit surface area at the level of the ceiling, is given by:

$$\dot{h}_{net} = \dot{h} - \alpha_c \cdot (\theta_m - 20) - \phi \cdot \varepsilon_m \cdot \varepsilon_f \cdot \sigma \cdot [(\theta_m + 273)^4 - 293^4] \qquad (2.14)$$

$\dot{h}$ - heat flux received by the fire exposed unit surface area at level of the ceiling [W/m^2] ;
α_c - the coefficient of heat transfer by convection [W/m^{2}K];
ϕ - the configuration factor [-];
θ_m - the surface temperature of the member [°C];
ε_m - the surface emissivity of the member [-];
ε_f - the emissivity of the fire [-];
σ - the Stephan Boltzmann constant (=5.67·10^{-8} W/m^{2}K^4).

For simple fire models [10] recommends to take the coefficient of heat transfer by convection as $\alpha_c = 35$ W/m^{2}K. The surface emissivity for the carbon steel profiles is specified by [24] as $\varepsilon_m = 0.7$ (however the value 0.8 is taken for all calculations) and the emissivity of the fire according to [10] $\varepsilon_f = 1.0$. The configuration factor could be conservatively taken as $\phi = 1.0$. However, annex G in [10] gives the method for the calculation of the configuration factor.

The vertical position of the virtual heat source z' comes from Hasemi's fire description in which a fire plume is idealised as an invert cone. At the bottom there is a point source fire and with moving upwards the cone expands. The position of the virtual origin depends on the diameter of the fire and the heat release rate. It can be above the base of the fire or below (negative value). In the latter case it indicates that the energy being released over the fire area is relatively small compare to the size of that area [25].

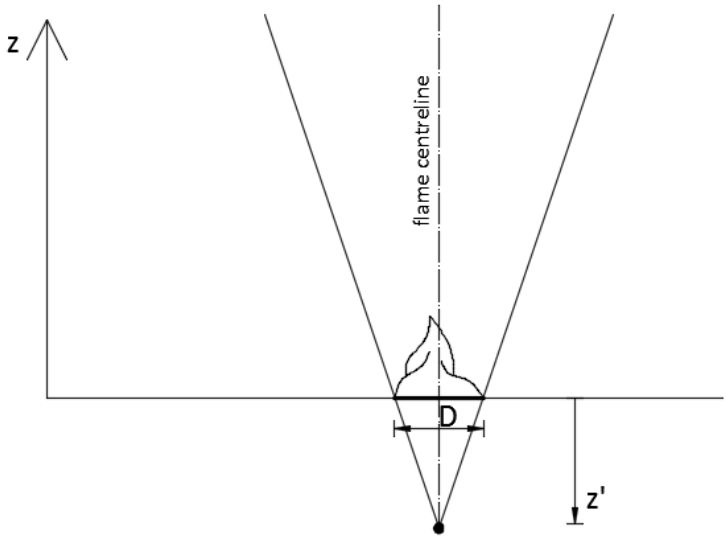

Figure 5. Hasemi fire description

2.4 Overview of radiation models

Thermal radiation is a phenomenon of heating up an object which is not in a direct contact with a fire. Thermal radiation relies on transferring the energy by electromagnetic waves which are emitted from very small particles. These soot particles are present in almost all diffusion flames and give a characteristic yellow luminance to the flame [26]. The total emissive power was described in 1901 by Max Planck as a function of temperature and wavelength. It was defined for an ideal radiator, so called "black body". However, in reality the energy emitted by surfaces is less than that for the ideal radiator. The fraction of the emitted radiation out of the total possible emission is termed emissivity, ε [27]. The maximum value of the emissivity equals to unit and refers to the "black body". Drysdale [26] introduced a concept of a "grey body" which assumes that the emissivity is independent of wavelength. Therefore, the total radiation emitted from a grey surface can be expressed by:

$$E = \varepsilon \, \sigma \, T_f^4 \tag{2.15}$$

Where:

- ε - the flame emissivity [-];
- σ - the Stefan-Boltzman constant (=5.67 x 10^{-8} W/m^{2}K^4);
- T_f - the flame temperature [K].

The total emissive power of the flame which is given by the equation above, defines the radiative heat loss from a unit area. However, to calculate the radiative heat flux received by fire exposed object, the energy radiated in that particular direction has to be calculated. So that, a concept of a configuration factor is introduced:

$$\dot{q}'' = F_{1\to 2} \, E \tag{2.16}$$

Where $\dot{q}''$ is the thermal radiation flux and $F_{1\to 2}$ is a geometric view factor, also called configuration factor or shape factor.

2.4.1 Shokri and Beyler model

Shokri and Beyler [28] method is based on a common "solid flame" radiation model. This approach assumes that the fire is a solid vertical cylinder emitting thermal radiation from the sides at an averaged rate of emissive power over the flame height of the fire. The radiative heat flux is expressed by Equation 2.16 Based on experimental tests, Shokri and Beyler give the following formula for the flame emissive power expressed in terms of the effective diameter:

$$E = 58 \, (10^{-0.00823D}) \tag{2.17}$$

The emissive power decreases with increasing pool diameter. The expression takes into account the smoke which obscures the thermal radiation from the luminous flame. The effective fire diameter in case of non-circular fires is calculated from:

$$D = \sqrt{\frac{4A_f}{\pi}} \tag{2.18}$$

where A_f is the fire area. However, this method is valid for fires with length to width aspect ratio close to 1. The flame height of the pool fire is determined from Heskestad correlation [29]:

$$H_f = 0.235\dot{Q}^{\frac{2}{5}} - 1.02D \tag{2.19}$$

Shokri and Beyler's approach takes into account the wind conditions and also the height of the target. If the target is on the ground floor or at the level of the top of the flame, only one cylinder is used to represent the flame. If the target is placed on the height between the ground level and the top of the flame, two cylinders represent the flame (Figure 6).

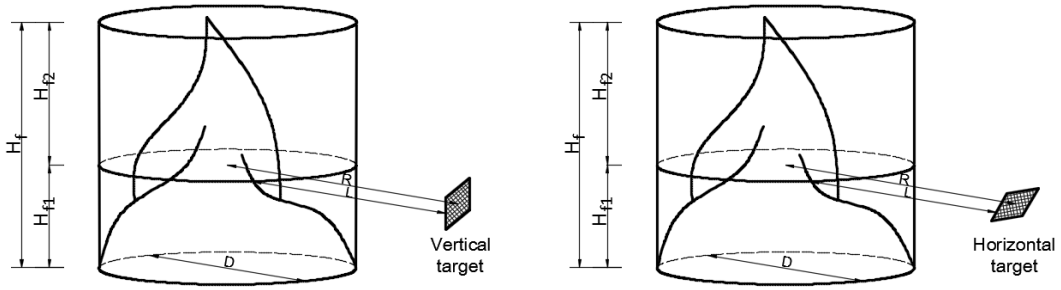

Figure 6. Solid model presented by Shokri and Beyler

For horizontal target orientation and still wind conditions, the configuration factor is as presented below:

$$F_{1\to 2,H} = \left(\frac{(B - \frac{1}{S})}{\pi\sqrt{B^2 - 1}} tan^{-1} \sqrt{\frac{(B+1)(S-1)}{(B-1)(S+1)}} - \frac{(A - \frac{1}{S})}{\pi\sqrt{A^2 - 1}} tan^{-1} \sqrt{\frac{(A+1)(S-1)}{(A-1)(S+1)}} \right) \tag{2.20}$$

For vertical target orientation and also no-wind conditions, the configuration factor is:

- At the ground level

$$F_{1\to 2,V} = \left(\frac{1}{\pi S} tan^{-1}\left(\frac{h}{\sqrt{S^2-1}}\right) - \frac{h}{\pi S} tan^{-1}\sqrt{\frac{S-1}{S+1}} + \frac{Ah}{\pi S\sqrt{A^2-1}} tan^{-1}\sqrt{\frac{(A+1)(S-1)}{(A-1)(S+1)}} \right) \quad (2.21)$$

Where:

$$R = L + 0.5D \quad (2.22)$$

$$A = \frac{h^2 + S^2 + 1}{2S} \quad (2.23)$$

$$B = \frac{1 + S^2}{2S} \quad (2.24)$$

$$S = \frac{2R}{D} \quad (2.25)$$

$$h = \frac{2H_f}{D} \quad (2.26)$$

and

L - the distance between the center of the cylinder (flame) to the target [m];

H_f - the height of the cylinder (flame) [m];

D - the cylinder (flame) diameter [m].

The maximum configuration factor is the vectorial sum of the horizontal and vertical view factors

$$F_{1\to 2,\max(no-wind)} = \sqrt{F_{1\to 2,H}^2 + F_{1\to 2,V}^2} \quad (2.27)$$

- Above the ground (two cylinders are used to represent the flame) (Figure 6)

$$F_{1\to 2,V_1} = \left(\frac{1}{\pi S} tan^{-1}\left(\frac{h_1}{\sqrt{S^2-1}}\right) - \frac{h_1}{\pi S} tan^{-1}\sqrt{\frac{S-1}{S+1}} + \frac{A_1 h_1}{\pi S\sqrt{A_1^2-1}} tan^{-1}\sqrt{\frac{(A_1+1)(S-1)}{(A_1-1)(S+1)}} \right) \tag{2.28}$$

$$S = \frac{2R}{D} \tag{2.29}$$

$$h_1 = \frac{2H_{f1}}{D} \tag{2.30}$$

$$A_1 = \frac{h_1^2 + S^2 + 1}{2S} \tag{2.31}$$

$$F_{1\to 2,V_2} = \left(\frac{1}{\pi S} tan^{-1}\left(\frac{h_2}{\sqrt{S^2-1}}\right) - \frac{h_2}{\pi S} tan^{-1}\sqrt{\frac{S-1}{S+1}} + \frac{A_2 h_2}{\pi S\sqrt{A_2^2-1}} tan^{-1}\sqrt{\frac{(A_2+1)(S-1)}{(A_2-1)(S+1)}} \right) \tag{2.32}$$

$$h_2 = \frac{2H_{f2}}{D} \tag{2.33}$$

$$A_2 = \frac{h_2^2 + S^2 + 1}{2S} \tag{2.34}$$

The total vertical configuration factor is expressed as the sum of two configuration factors

$$F_{1\to 2,\mathrm{V}(no-wind)} = F_{1\to 2,\mathrm{V}\,1} + F_{1\to 2,\mathrm{V}\,2} \tag{2.35}$$

Horizontal targets require only one equation. It is assumed that the subject receives radiation only on one side. It is necessary to specify if it is downwards-facing surface or upwards-facing surface. Then the equation for the horizontal target orientation at the ground level has to be employed using cylinder 1 or cylinder 2, respectively [30].

2.4.2 Mudan and Croce model

Mudan and Croce method is also based on the assumption of cylindrical in shape flame and an averaged rate of emissive power over the flame height [28]. It can be applied to circular or nearly circular in shape fires after calculating the effective diameter from Equation 2.18. The radiative heat flux is also given by Equation 2.16. For still air investigation, the flame height is calculated from Thomas correlation [31]:

$$\frac{H}{D} = 42\left(\frac{\dot{m}''}{\rho_a\sqrt{gD}}\right)^{0.61} \tag{2.36}$$

and the view factor from Equations 2.20-2.35. The effective emissive power is determined from:

$$E = E_{max}e^{(-sD)} + E_s(1 - e^{(-sD)}) \tag{2.37}$$

Where E_{max} is the equivalent black body emissive power (140 kW/m^2), s is the extinction coefficient (0.12 m^{-1}) and E_s represents the emissive power of smoke (20 kW/m^2), as given by Beyler [32].

Mudan [33] gives formulas to consider wind in radiative heat flux calculations. Under wind conditions the flame is also approximated by a cylinder but not vertical anymore only angled at θ (Figure 7). The expressions below can be used for the target at the ground level.

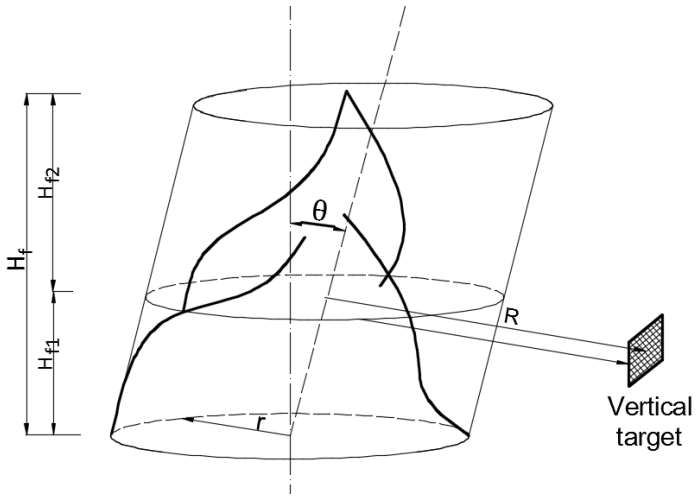

Figure 7. Solid flame model under wind conditions

$$\pi F_{1\to 2,H} = \left(tan^{-1}\sqrt{\frac{b+1}{b-1}} - \frac{a^2+(b+1)^2-2(b+1+absin\theta)}{\sqrt{AB}} tan^{-1}\sqrt{\frac{A}{B}}\sqrt{\frac{(b-1)}{(b+1)}} + \frac{sin\theta}{\sqrt{C}}\left(tan^{-1}\frac{ab-(b^2-1)sin\theta}{\sqrt{b^2-1}\sqrt{C}} + tan^{-1}\frac{(b^2-1)sin\theta}{\sqrt{b^2-1}\sqrt{C}} \right) \right) \quad (2.38)$$

$$\pi F_{1\to 2,V} = \left(\frac{acos\theta}{b-asin\theta}\frac{a^2+(b+1)^2-2b(1+asin\theta)}{\sqrt{AB}} tan^{-1}\sqrt{\frac{A}{B}}\sqrt{\frac{(b-1)}{(b+1)}} + \frac{cos\theta}{\sqrt{C}}\left(tan^{-1}\frac{ab-(b^2-1)sin\theta}{\sqrt{b^2-1}\sqrt{C}} + tan^{-1}\frac{(b^2-1)sin\theta}{\sqrt{b^2-1}\sqrt{C}} \right) - \frac{acos\theta}{(b-asin\theta)} tan^{-1}\sqrt{\frac{(b-1)}{(b+1)}} \right) \quad (2.39)$$

Where:

$$a = \frac{H_f}{r} \quad (2.40)$$

$$b = \frac{R}{r} \quad (2.41)$$

$$A = a^2 + (b+1)^2 - 2a(b+1)sin\theta \quad (2.42)$$

$$B = a^2 + (b-1)^2 - 2a(b-1)sin\theta \quad (2.43)$$

$$C = 1 + (b^2-1)cos^2\theta \quad (2.44)$$

Similar as for still air flame model, the maximum configuration factor at a point is the vectorial sum of the horizontal and vertical view factors:

$$F_{1\to 2,\max(wind)} = \sqrt{F_{1\to 2,H}^2 + F_{1\to 2,V}^2} \quad (2.45)$$

For targets above ground level, following formulas are used with the distinction for the cylinder 1 below the target and cylinder 2 above the point of interest:

$$\pi F_{1\to 2,V1} = \left(\frac{a_1 cos\theta}{b - a_1 sin\theta} \frac{a_1^2 + (b+1)^2 - 2b(1 + a_1 sin\theta)}{\sqrt{AB}} tan^{-1} \sqrt{\frac{A_1}{B_1}} \sqrt{\frac{(b-1)}{(b+1)}} + \frac{cos\theta}{\sqrt{C}} \left(tan^{-1} \frac{a_1 b - (b^2-1) sin\theta}{\sqrt{b^2-1}\sqrt{C}} + tan^{-1} \frac{(b^2-1) sin\theta}{\sqrt{b^2-1}\sqrt{C}} \right) - \frac{a_1 cos\theta}{(b - a_1 sin\theta)} tan^{-1} \sqrt{\frac{(b-1)}{(b+1)}} \right) \quad (2.46)$$

$$\pi F_{1\to 2,V2} = \left(\frac{a_2 cos\theta}{b - a_2 sin\theta} \frac{a_2^2 + (b+1)^2 - 2b(1 + a_2 sin\theta)}{\sqrt{AB}} tan^{-1} \sqrt{\frac{A_2}{B_2}} \sqrt{\frac{(b-1)}{(b+1)}} + \frac{cos\theta}{\sqrt{C}} \left(tan^{-1} \frac{a_2 b - (b^2-1) sin\theta}{\sqrt{b^2-1}\sqrt{C}} + tan^{-1} \frac{(b^2-1) sin\theta}{\sqrt{b^2-1}\sqrt{C}} \right) - \frac{a_2 cos\theta}{(b - a_2 sin\theta)} tan^{-1} \sqrt{\frac{(b-1)}{(b+1)}} \right) \quad (2.47)$$

Where:

$$a_1 = \frac{2H_{f1}}{r} = \frac{2H_1}{r} \quad (2.48)$$

$$a_2 = \frac{2H_{f2}}{r} = \frac{2(H_f - H_{f1})}{r} \quad (2.49)$$

$$b = \frac{R}{r} \quad (2.50)$$

$$A_1 = a_1^2 + (b+1)^2 - 2a_1(b+1) sin\theta \quad (2.51)$$

$$A_2 = a_2^2 + (b+1)^2 - 2a_2(b+1) sin\theta \quad (2.52)$$

$$B_1 = a_1^2 + (b-1)^2 - 2a_1(b-1) sin\theta \quad (2.53)$$

$$B_2 = a_2^2 + (b-1)^2 - 2a_2(b-1) sin\theta \quad (2.54)$$

$$C = 1 + (b^2 - 1) cos^2\theta \quad (2.55)$$

Under wind conditions following Thomas expression allows to estimate the flame height [31]:

$$H_f = 55D \left(\frac{\dot{m}''}{\rho_a \sqrt{gD}} \right)^{0.67} (u^*)^{-0.21} \quad (2.56)$$

Where:

D	-	the diameter of pool fire [m];
$\dot{m}''$	-	the mass burning rate of fuel [kg/m^{2}s];
ρ_a	-	the ambient air density [kg/m^3];
g	-	the gravitational acceleration [m/s^2];
u*	-	the non-dimensional wind velocity [-].

The non-dimensional wind velocity is expressed by:

$$u^* = \frac{u_w}{\left(\frac{g\dot{m}''D}{\rho_a}\right)^{1/3}} \tag{2.57}$$

Where u_w is the wind velocity in m/s. The American Gas Association (AGA) data gives the correlation related to angle of tilt as follows [34]:

$$cos\theta = \begin{cases} 1 & \text{for} \quad u^* \leq 1.0 \\ \frac{1}{\sqrt{u^*}} & \text{for} \quad u^* \geq 1.0 \end{cases} \tag{2.58}$$

2.4.3 Modified Solid Flame Model

National Institute of Standards and Technology (NIST) presents also the methodology to calculate the thermal radiation flux [35]. This method is intended for large fires of combustible liquids and gases and emends the existing methods considering the effect of smoke on the radiation. The shielding effect occurs in case of high diameter fires, which characterise in generating an appreciable amount of smoke due to less efficient combustion compare with small fires. The smoke covers much of the luminous flame region and blocks the radiation.

Former methodology is described in the 1975 HUD guidelines [36] and it assumes that fire is unobscured by smoke what leads in some scenarios to overestimating the radiation flux. The modified method is based on additional studies involving the effect of the fire size and radiant intensity on the radiation. Nonetheless, approach presented by NIST assumes the same solid flame model as methods described before.

The method given in the 1975 HUD guidelines considered the view factor and the total emissive power individually. In some cases, this approach gave higher thermal radiation than the total energy of the fire. This problem was solved by overall accounting of energy by introducing the

heat release rate (HRR). HRR is proportional to the mass burning rate which can be easily obtained from fire experiments and the thermal radiation is a fraction of the total HRR.

More generally, the energy radiated from the fire can be expresses with the perimeter P as follows:

$$\chi_r \dot{Q} = P\ H\ E \tag{2.59}$$

The fraction of the thermal radiation is between 0.3 and 0.4 for the fires up to 4.0 m in diameter and decreases for the larger fires, according to the formula:

$$\chi_r = \chi_{r,max} e^{-kD} \tag{2.60}$$

where $\chi_{r,max} = 0.35$ and $k = 0.05\ m^{-1}$ based on the experimental data. The total HRR of the fire is the product of the heat release rate per unit area $\dot{q}_f{''}$ and the area of the base of the fire A_f:

$$\dot{Q} = \dot{q}_f{''} A_f \tag{2.61}$$

There are two approaches to predict thermal radiation from large fires. One method assumes an average emissive power over the flame height. This assumption is made for Shokri and Beyler model, as well as Mudan and Croce model, what was presented before. The second method refers only to the height of the luminous zone H (lower than the total height of the flame). This assumption is made for the modified solid flame model given by NIST. The flame region above the luminous zone is shielded by the smoke and slightly contributes to the thermal radiation (Figure 8). In this case, a constant emissive power equal to $100\ kW/m^2$ is taken. From the above formulas the height of the luminous flame zone can be found:

$$H = \frac{\chi_{r,max} e^{-kD}\ \dot{Q}}{P\ E} \tag{2.62}$$

Approach given by NIST is aimed to determine the Acceptable Separation Distance (ASD). According to [37]: *Acceptable separation distance (ASD) – means the distance beyond which the explosion or combustion of a hazard is not likely to cause structures or individuals to be subjected to blast over-pressure or thermal radiation flux levels in excess of the safety standards.*

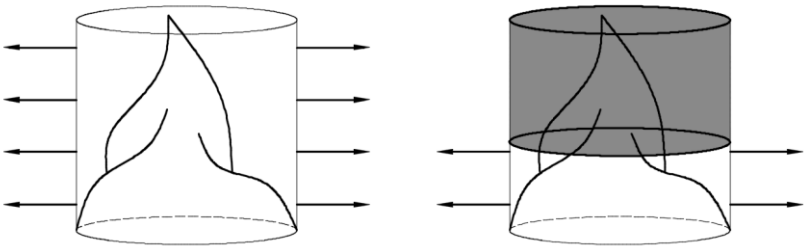

Figure 8. Solid flame models: Average emissive power over the flame height (left), Emissive power over the luminous zone (right)

In case of the buildings situated nearby combustible liquids, within the ASD distance the thermal radiative flux should be smaller than 31.5 kW/m^2. For people, the threshold is much lower and equals to 1.4 kW/m^2 [37].

There are two calculation methods available for hazardous liquids. If the fuel is liquid at atmospheric temperature, if the fire is roughly circular around its base, and if there are no obstructions to be considered, simplified chart can be used (Figure 9). If any of the given criteria are not met, detailed calculations are required.

The simplified chart is based on the assumption that the bottom of the fire is a circle. Otherwise, an equivalent fire diameter has to be specified as it was before. However, the threshold for the length to width ratio is 2.5 what is much higher than for the models described before.

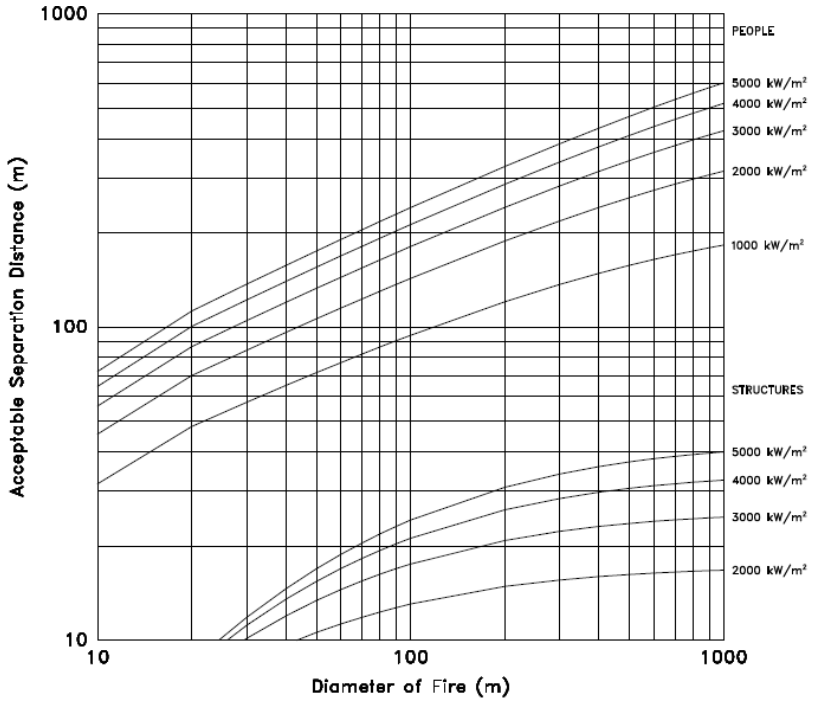

Figure 9. Acceptance Separation Distance (ASD) from nearby cylindrical fires resulting from spills of hazardous liquids [35]

Detailed calculation enables the direct calculation of the thermal radiation flux at a particular location from the Equation 2.16. As mentioned before, the emissive power E is considered to be 100 kW/m^2. The view factor is calculated by assuming that the fire is separated from a target by a vertical plate of width W and height H, emitting energy at a rate of E (Figure 10). To calculate the view factor for the target at the distance S from the centre of the plate and S' from the centreline, the expression below and Table 2 are used.

$$F(S,S',H,W)=\begin{cases}\dfrac{F(S,0,H,2S'+W)-F(S,0,H,2S'-W)}{2} & 2S'>W\\ \dfrac{F(S,0,H,2S'+W)+F(S,0,H,W-2S')}{2} & 2S'<W\end{cases} \tag{2.63}$$

Table 2. View factors from a flat vertical plate [30]

S/W	H/W																		
	0.01	0.02	0.03	0.04	0.05	0.06	0.07	0.08	0.09	0.1	0.2	0.3	0.4	0.5	0.6	0.7	0.8	0.9	1
0.1	0.050	0.098	0.143	0.185	0.223	0.256	0.286	0.311	0.333	0.352	0.444	0.470	0.480	0.484	0.486	0.488	0.489	0.489	0.489
0.2	0.024	0.049	0.072	0.096	0.118	0.140	0.161	0.181	0.200	0.218	0.343	0.401	0.428	0.442	0.450	0.455	0.457	0.459	0.461
0.3	0.016	0.031	0.047	0.062	0.077	0.092	0.106	0.120	0.134	0.148	0.257	0.325	0.364	0.387	0.401	0.409	0.415	0.418	0.421
0.4	0.011	0.022	0.033	0.044	0.055	0.065	0.076	0.086	0.096	0.107	0.195	0.259	0.302	0.330	0.348	0.360	0.368	0.373	0.377
0.5	0.008	0.016	0.024	0.033	0.041	0.049	0.057	0.065	0.072	0.080	0.151	0.206	0.248	0.277	0.298	0.312	0.322	0.329	0.335
0.6	0.006	0.013	0.019	0.025	0.031	0.038	0.044	0.050	0.056	0.062	0.118	0.166	0.203	0.232	0.253	0.269	0.281	0.289	0.296
0.7	0.005	0.010	0.015	0.020	0.025	0.030	0.035	0.039	0.044	0.049	0.095	0.135	0.168	0.195	0.216	0.232	0.244	0.253	0.261
0.8	0.004	0.008	0.012	0.016	0.020	0.024	0.028	0.032	0.036	0.040	0.077	0.111	0.140	0.164	0.184	0.200	0.212	0.222	0.230
0.9	0.003	0.007	0.010	0.013	0.016	0.020	0.023	0.026	0.029	0.033	0.064	0.093	0.118	0.140	0.158	0.173	0.185	0.195	0.203
1.0	0.003	0.005	0.008	0.011	0.014	0.016	0.019	0.022	0.025	0.027	0.054	0.078	0.100	0.120	0.136	0.151	0.162	0.172	0.180
2.0	0.001	0.002	0.002	0.003	0.004	0.005	0.005	0.006	0.007	0.008	0.015	0.023	0.030	0.037	0.043	0.050	0.056	0.061	0.066
3.0	0.000	0.001	0.001	0.001	0.002	0.002	0.002	0.003	0.003	0.003	0.007	0.010	0.014	0.017	0.020	0.023	0.027	0.030	0.032
4.0	0.000	0.000	0.001	0.001	0.001	0.001	0.001	0.002	0.002	0.002	0.004	0.006	0.008	0.010	0.012	0.014	0.015	0.017	0.019
5.0	0.000	0.000	0.000	0.001	0.001	0.001	0.001	0.001	0.001	0.001	0.003	0.004	0.005	0.006	0.008	0.009	0.010	0.011	0.012
6.0	0.000	0.000	0.000	0.000	0.000	0.001	0.001	0.001	0.001	0.001	0.002	0.003	0.004	0.004	0.005	0.006	0.007	0.008	0.009
7.0	0.000	0.000	0.000	0.000	0.000	0.000	0.000	0.001	0.001	0.001	0.001	0.002	0.003	0.003	0.004	0.005	0.005	0.006	0.006
8.0	0.000	0.000	0.000	0.000	0.000	0.000	0.000	0.000	0.000	0.000	0.001	0.001	0.002	0.002	0.003	0.003	0.004	0.004	0.005
9.0	0.000	0.000	0.000	0.000	0.000	0.000	0.000	0.000	0.000	0.000	0.001	0.001	0.002	0.002	0.002	0.003	0.003	0.004	0.004
10.0	0.000	0.000	0.000	0.000	0.000	0.000	0.000	0.000	0.000	0.000	0.001	0.001	0.001	0.002	0.002	0.002	0.003	0.003	0.003

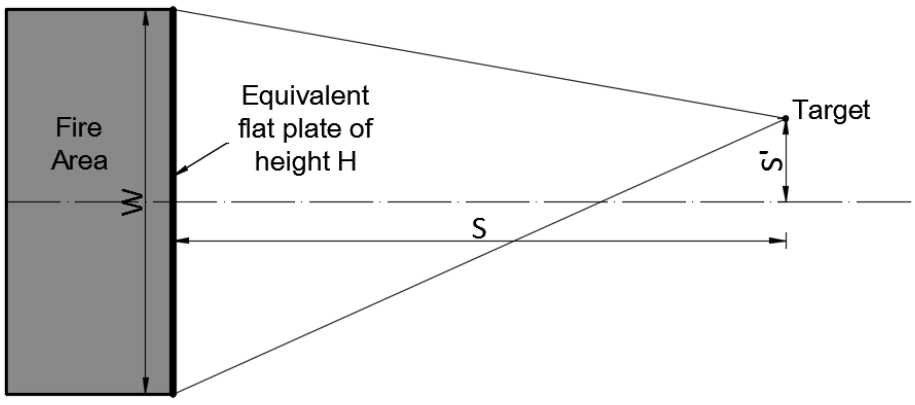

Figure 10. Notation used in view factor calculations

2.4.4 Rectangular Planar Model

All models described before are based on the assumption that the flame is cylindrical in shape so the effective diameter is calculated. This is common situation for tanks of circular cross section which are used to store liquid fuels. In compartments fire is usually related to burning furniture so the base of the fire is usually not circular. Also in this study the fire area is always rectangular in shape so better assumption would be to assume that the flame is cuboid. A rectangular based model approximates the flame as two perpendicular intersecting planes - α and β (Figure 11). The configuration factors are determined for each plane and the total shape factor is the sum of these two components [30].

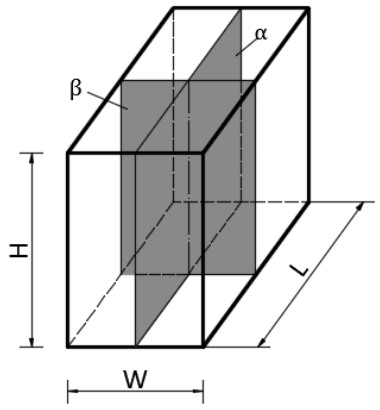

Figure 11. Rectangular Planar Model

To calculate the shape factor for receiving plane which is paraller to the radiating surface, the Howell formula can be applied [38]:

$$F_{1\to 2} = \frac{1}{2\pi}\left[\frac{a}{\sqrt{1+a^2}}tan^{-1}\left(\frac{b}{\sqrt{1+a^2}}\right) + \frac{b}{\sqrt{1+b^2}}tan^{-1}\left(\frac{a}{\sqrt{1+b^2}}\right)\right] \quad (2.64)$$

Where:

$$a = \frac{H}{R} \quad (2.65)$$

$$b = \frac{L}{R} \quad (2.66)$$

It accounts when the normal from the radiating plane to the target passes its corner. R is the distance from the centre of the fire to the target. More details about this approach are given in annex G in [10].

3. CASE STUDY

3.1 Description of the offshore structure

In this thesis the case study corresponds to a "fictitious" fixed offshore platform, which dimensions are based on the typical offshore platforms. It is defined as an open structure, composed by three primary decks: cellar deck, main deck and top deck. Mezzanine deck and intermediate deck are two secondary floors placed between the cellar and main decks and the main and top decks, respectively (Figure 12).

The decks consist of primary beams being made of steel profiles. Between the main beam grids, stringers with steel profiles are welded, to provide the support for plated steel decks. The main floor decks are of steel plates. The intermediate decks are characterized by grated steel plates.

The integration of the legs with the topside is made by four sleeve sections incorporated between the top deck and the main deck, at the corners of the topside.

An open space left between B and C rows is intended for the crane and other equipment and installation needed during the extraction of the fuel (Figure 13).

There are compartments between the main deck and the top deck and the refuge compartment on the top of the platform. This room is aimed at protecting personnel during a catastrophic event. Next to the temporary compartment, between row F and G, the muster area is situated (Figure 13). The topside also features a helideck on the east face.

3.2 Fire scenarios

The fire scenarios examined in this study assume an accidental crude oil release on the first level of the topside and resulting in a localised pool fire. The point is to compare the FDS field models with the available analytical methods. As mentioned before, they can be applied only within some limitations. In total there are 6 scenarios: Scenario 1, Scenario 2, Scenario 3A, Scenario 3B, Scenario 4A and Scenario 4B. The difference between them is in the fire area and the wind conditions, as presented in Table 3 and Figures 14-17.

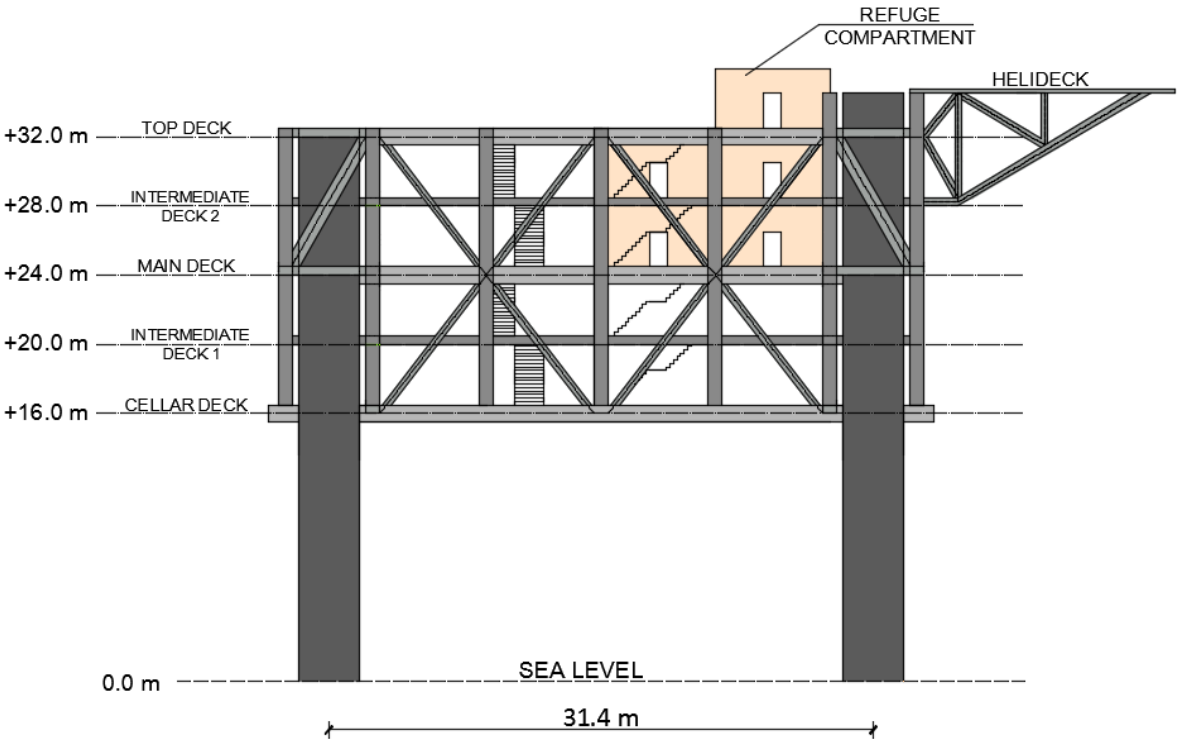

Figure 12. Side view of the study case

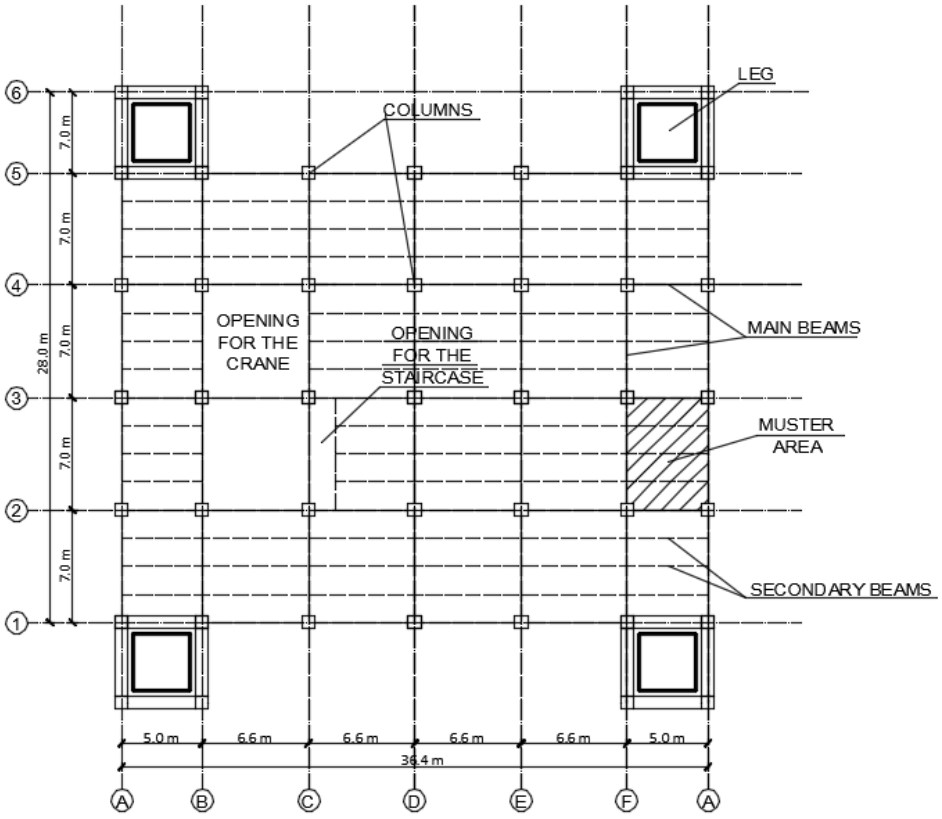

Figure 13. View on the top deck

HRRPUA is based on the Babrauskas data and considers Blinov and Khudiakov proposal, what is explained in section 3.3.2.

Methods presented in EN 1991-1-2 are mostly aimed at compartment fires, limited by the size and the geometry. A simplified calculation model can be used for open air fires to assess localized fires. However, this method is not applicable for the fire affected by wind. In addition, the diameter of the fire area has to be smaller than 10 m and the heat release rate should not exceed 50 MW. The two last conditions limit examined fire area for crude oil to 26 m^2 [10]. From this reason, to verify the model with methods available in Eurocode, Scenario 1 and Scenario 2 are considered. The difference between them is embedded in the fire area. It results in use of the Heskestad approach and the Hasemi method, respectively, as it is explained in section 2.3.

Scenario 3 and Scenario 4 are typical large pool fires, much more severe in comparison with Scenario 1 and Scenario 2. In this case, they are studied by radiation models presented in section 2.4. The examined radiation models are based on the assumption that the flame is cylindrical in shape. The effective diameter should be determined for fire areas rectangular in shape. The closest to unit length-to-width ratio for the fire base, the best approximation of the circle. In case of Scenario 3 mentioned ratio equals 1.2 however, for Scenario 4, it is 2.3. Moreover, the effect of the wind is also studied.

Table 3. Fire scenarios

	Scenario 1	**Scenario 2**	**Scenario 3**		**Scenario 4**	
Width, W [m]	2.0	6.4	6.4		6.4	
Length, L [m]	2.0	4.0	7.4		14.8	
Total fire area, A_f [m^2]	4.0	25.6	47.4		94.7	
Case	**-**	**-**	**A**	**B**	**A**	**B**
Wind velocity, v [m/s]	0.0	0.0	0.0	5.0	0.0	5.0
HRRPUA [kW/m^2]	1920.0	1920.0	1920.0	2050.0	1920.0	2050.0
Total HRR [MW]	7.7	49.2	90.9	97.1	181.9	194.2

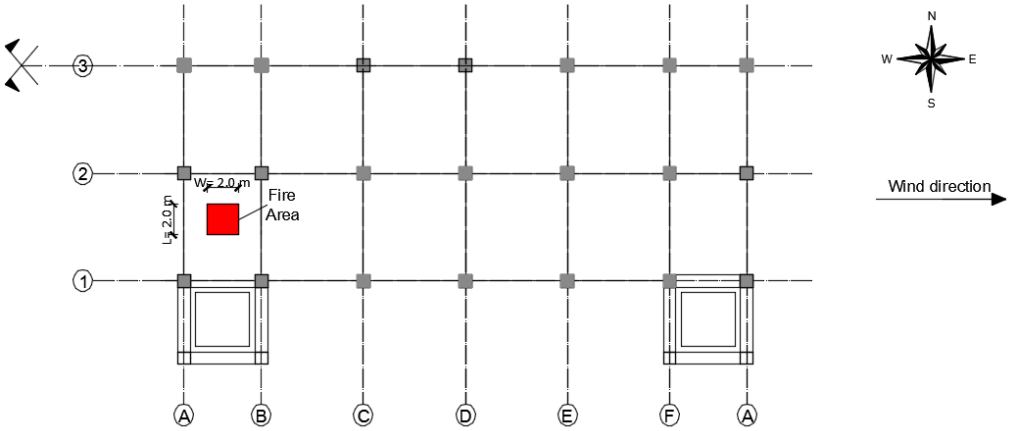

Figure 14. Fire scenario 1

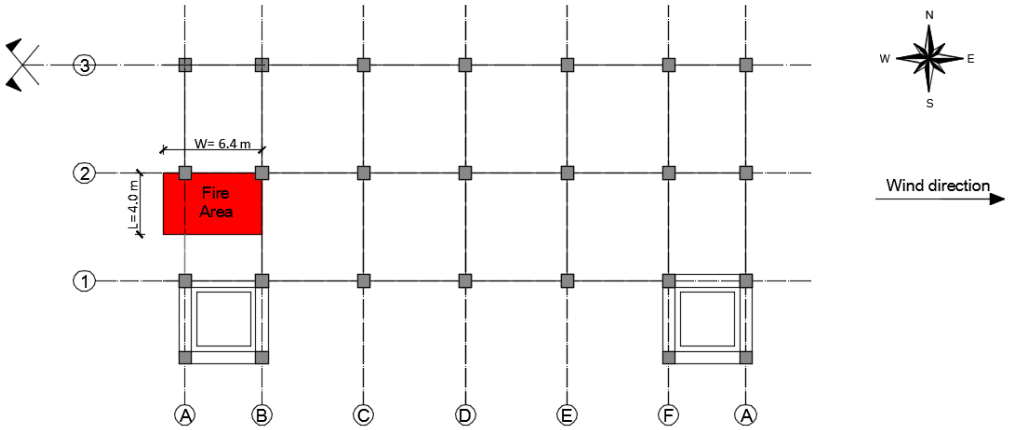

Figure 15. Fire scenario 2

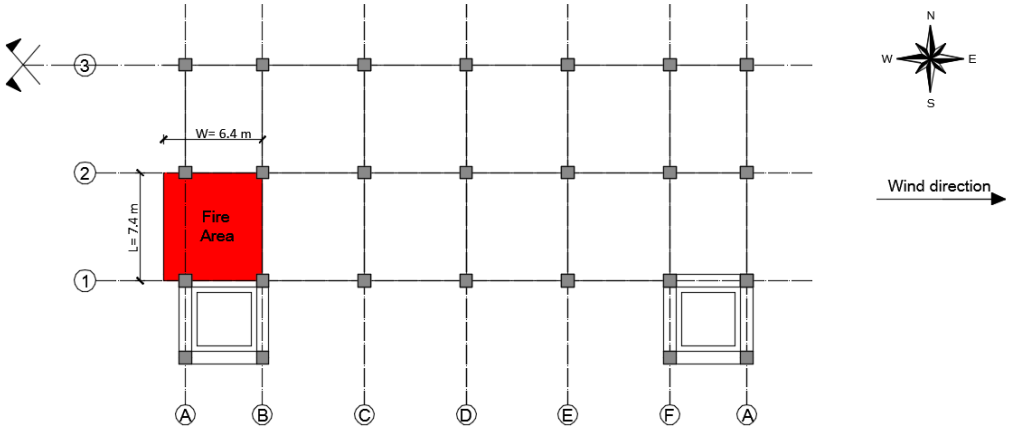

Figure 16. Fire scenario 3 (A and B)

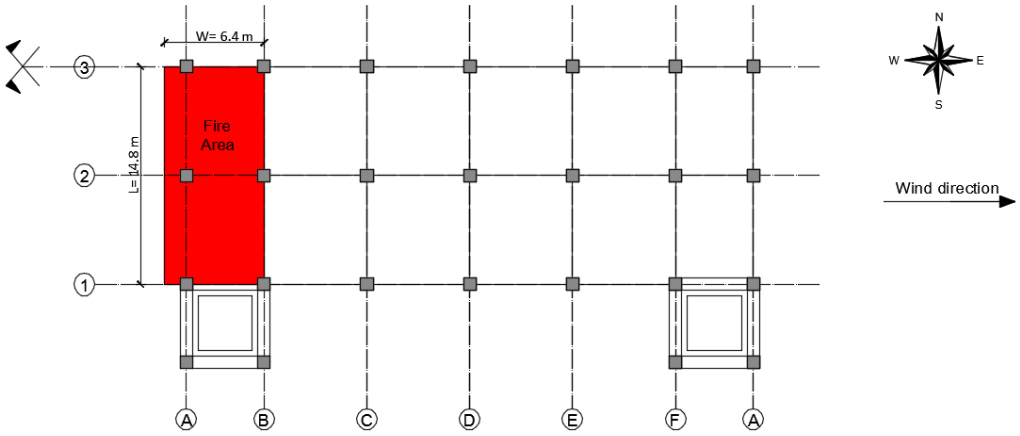

Figure 17. Fire scenario 4 (A and B)

3.3 Numerical modelling

3.3.1 General requirements for the definition of the numerical model in FDS

The robustness and accuracy of FDS requires a fast CPU, satisfying amount of RAM and a large hard drive to store the output files. Running the model can take days or even weeks. It depends on the computer or whether the parallel processing is performed. The run time highly depends on the total grid number. To decrease CPU time, symmetrical model is assumed. It allows halve the domain. Moreover, considering that the fire starts on the first level of the topside, the space between the cellar deck and the sea level is omitted (Figure 18). For considered fire scenarios, it is expected that the impact of the fire on the helicopter landing deck will be less severe than on the muster area so this part is not included in the model. Finally, the dimension of the computational domain is 44.0 m by 22.8 m by 23.6 m (Figure 18). This domain will be called in this study “full domain” because in some cases it will be reduced.

Faces of obstructions in FDS are shifted to the closest mesh cell. It means that the geometry is adapted to the grid cell size. Since the mesh elements are cubic, the geometry of the structure is made up entirely of these cubes of different sizes, depending on the grid resolution. This makes some limitations in defining circular sections, diagonal bracing or thin obstacles. For example, the legs and columns are modelled with large squared cross-sections.

Additionally, when smoke development is under consideration it is important to reflect as realistically as possible the grated surfaces. Even if the empty space is not comparable with the used grid cell size, the conservative approach is not to draw the grated object at all, what was done in this model in case of the intermediate decks.

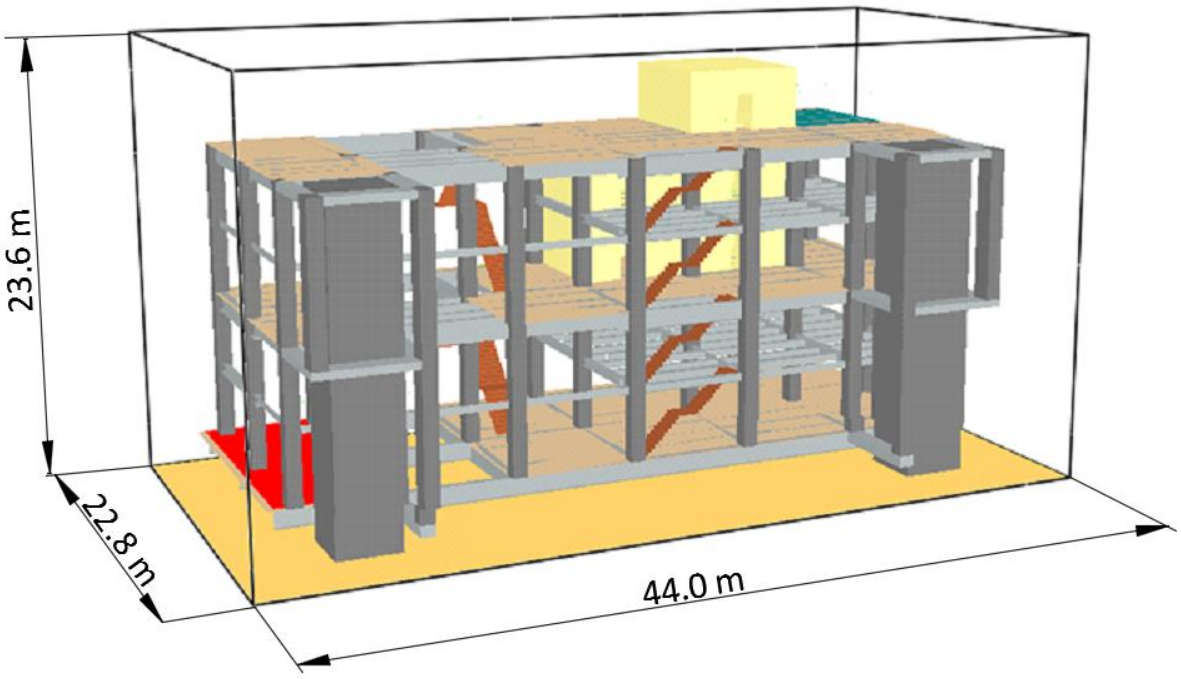

Figure 18. The numerical model of offshore platform and its computational domain in FDS

3.3.2 Presentation and explanation of the input data

Numerical modelling is based on assumptions which should in the best possible way reflect the reality. The model should be as simple as possible to obtain reliable results with the least effort. All models require a good justification, proper assumptions but also a correct interpretation. Wrong parameters may lead to the lack of sufficient conservatism or even discrepant results. Therefore, designers should take the opportunity from previous researches, experiments and their own experience. It is hard to say that assumptions made in favour of this thesis are based on experience but they were carefully selected by reviewing available sources.

Heat release rate

The most common fire that occurs on the offshore platforms is hydrocarbon pool fire. It is an open-topped fire, usually the result of spilled hydrocarbon fuels on the deck structure. Significant parameter of the fire is the fire burning rate. Simply, it indicates how fast the fire burns. Babrauskas has summarized the available information for large pool fires ($D \geq 0.2$ m). As stated before, for large pool fires, radiative heat transfer dominates burning, as opposed to small diameter fires, which are driven by convection. Additionally, in the convective dominated fires, the flow can be either laminar or turbulent, while for radiative dominated fires it is always turbulent as shown in Table 4. [41].

Table 4. Distinction of the fire [41]

D [m]	Burning mode
< 0.05	convective, laminar
0.05-0.2	convective, turbulent
0.2-1.0	radiative, optically thin
>1.0	radiative, optically thick

Babrauskas [41] recommends calculate the burning rates of the large pool fires from the equations:

$$\dot{m}'' = \dot{m}''_{\infty}(1 - e^{-k\beta D}) \tag{3.3}$$

And

$$\dot{Q} = \Delta h_c \, \dot{m}'' \, A \tag{3.4}$$

Where:

$\dot{m}''$ - the pool mass loss rate [kg/m^{2}s];
$\dot{m}''_{\infty}$ - the infinite-diameter pool mass loss rate [kg/m^{2}s];
k - the extinction coefficient [m^{-1}];
β - the mean beam length corrector [-];
D - the pool diameter [m], $= \sqrt{4A_f/\pi}$ for noncircular pools;
$\dot{Q}$ - the total heat release rate [kW];
Δh_c - the lower heat of combustion [kJ/kg];
A - the pool area [m^2];

The same author presents tabulated data to estimate directly the burning rates of large pool fires. Nonetheless, he emphasises that the strong predictions are valid only for particular conditions. The largest uncertainties can be introduced due to wind effects. The values in Table 5 pertain to a wind-free environment. Unfortunately, it was observed that, for large-diameter pools exposed to wind, the burning rate increased. In Lous and Swiethenbank tests [42], it was even doubled for a hexane pool fire and 4m/s wind but there was no more increase for higher speeds. Blinov and Knudziakov [43] present formula:

$$\frac{\dot{m}''_{windy}}{\dot{m}''_{still}} = 1 + 0.15 \, \frac{v}{D} \tag{3.5}$$

which provides the most adequate solution so far. This expression is not appropriate for alcohol fuels and also for scenarios in which the high wind velocity can cause blow-off. It was observed for some fuels exposed to the wind velocity exceeding 5m/s.

Table 5. Data for Large Pool Burning Rate Estimates [41]

Material	Density [kg/m^3]	Δh_g [kJ/kg]	Δh_c [MJ/kg]	$\dot{m}''_\infty$ [kg/m^{2}s]	kβ [m^{-1}]	k [m^{-1}]	T_f [K]
Cryogenics							
Liguid H_2	700	442	120.0	0.1699 (±0.006)	6.1 (±0.4)	-	1600
LNG (mostly CH_4)	415	619	50.0	0.078 (±0.018)	1.1 (±0.8)	0.5	1500
LPG (mostly C_3H_8)	585	426	46.0	0.099 (±0.009)	1.4 (±0.5)	0.4	-
			Alcohols				
Methanol (CH_3OH)	796	1230	20.0	0.017 (±0.001)	-	-	1300
Ethanol (C_2H_5OH)	794	1000	26.8	0.015 (±0.001)	-	0.4	1490
Simple organic fuels							
Butane (C_4H_{10})	573	370	45.7	0.078 (±0.003)	2.7 (±0.3)	-	-
Benzene (C_6H_6)	874	500	40.1	0.085 (±0.002)	2.7 (±0.3)	4.0	1460
Hexane (C_6H_{14})	650	450	44.7	0.074 (±0.005)	1.9 (±0.4)	-	1300
Heptane (C_7H_{16})	675	505	44.6	0.101 (±0.009)	1.1 (±0.3)	-	-
Xylene (C_8H_{10})	870	555	40.8	0.090 (±0.007)	1.4 (±0.3)	-	-
Acetone (C_3H_6O)	791	570	25.8	0.041 (±0.003)	1.9 (±0.3)	0.8	-
Dioxane ($C_4H_8O_2$)	1035	530	26.2	0.018*	5.4*	-	-
Diethyl ether ($C_4H_{10}O$)	714	385	34.2	0.085 (±0.018)	0.7 (±0.3)	-	-
Petroleum Products							
Benzine	740	-	44.7	0.048 (±0.002)	3.6 (±0.4)	-	-
Gasoline	740	330	43.7	0.055 (±0.002)	2.1 (±0.3)	2.0	1450
Kerosene	820	670	43.2	0.039 (±0.003)	3.5 (±0.8)	2.6	1480
JP-4	760	-	43.5	0.051 (±0.002)	3.6 (±0.1)	-	1220
JP-5	810	700	43.0	0.054 (±0.002)	1.6 (±0.3)	0.5	1250
Transformer oil, hydrcarbon	760	-	46.4	0.039*	0.7*	-	1500
Fuel oil, heavy	940-1000	-	39.7	0.035 (±0.002)	1.7 (±0.6)	-	-
Crude oil	830-880	-	42.5-42.7	0.022-0.045	2.8 (±0.4)	-	-
Solids							
Polymethyl-methacrylate	1184	1611	24.9	0.020 (±0.002)	3.3 (±0.8)	1.3	1260

* Value independent of diameter in turbulent regime
* Only two data points available

Another problem with the use of tabulated data is related to the transient effects. In reality, a steady-state burning is not reached immediately after ignition. Transient effects need additional investigations to provide better estimates of burning rates; however they are still less significant compared with the wind effects.

Additionally, burning rate can be decreased as well. This effect was noticed for pool fires with very large diameters (D ≥ 5 or 10 m). Unfortunately, there are not enough experimental data in

this area arising from the costs of large scale experiments. Most likely the drop in the burning rate is due to poorer mixing but this effect should not be larger than 20% [41].

According to data given in Table 5 for the case with no wind HRRPUA = 1920 kW/m^2; while for 5 m/s wind velocity and considering Blinov and Khudiakov proposal: HRRPUA = 2050 kW/m^2.

Fuel

Crude oil is the only natural liquid fuel and it is a mixture of more than 3000 of hydrocarbons (C_mH_n) [44]. It is approximated to tetradecane which is a heavy hydrocarbon fuel with chemical formula $C_{14}H_{30}$ and molecular mass 198.39 g/mol.

Soot yield

There are several methods to measure the production of soot; however only those which capture or measure the soot entirely, give relatively precise values. A new technique during Newfoundland Offshore Burn Experiment (NOBE) uses airborne lidar which flies through the plume and maps the soot content [45]. A good navigation system enables to record the positions of the measured points and later to integrate the content of soot in smoke. The resulting downwind values for crude oil are 0.5 % and about 3% near the fire, what results in an average value 1.8 %. Technique in NOBE gives an error ranging between 0.28 and 2.5 %. In the study case the soot yield is assumed to be 2% [46]. It is a conservative value, as the increase in the soot yields the higher radiation.

Non-dimensional constant

A non-dimensional constant is an important factor which is used by software to calculate a visibility distance. It refers to optical properties of objects that are viewed through smoke. The non-dimensional constant can be taken as C = 3 for normally illuminated objects (light reflecting signs). This value is usually taken for places whose occupants are not familiar with the building. A value C = 8 is used for light emitting signs (backlit exit signs) [22]. In this case, the exits routes have to be well defined and people do not need to step around obstacles during evacuation. In the considered numerical model, the non-dimensional constant is taken as 3. Otherwise (C = 8), it would allow over 2.5 times more smoke in the space.

Materials

All beams and columns are made of steel profiles with the emissivity 0.8, the conductivity 45.0 W/mK and the specific heat 0.6 kJ/kgK. Compartments are modular enclosures made of sandwich panels: FRP (8 mm), gypsum board (12.7 mm), polystyrene foam (25.4 mm), gypsum board (12.7 mm), FRP (8 mm).

3.3.3 Grid resolution

Important aspect in terms of the run time and the accuracy of the results is the grid cell size. FDS User's Guide [22] suggests performing a mesh sensitivity study; this is done in the next section. The idea of this mentioned sensitivity analysis is to first run a model with a relatively coarse mesh, and then gradually decrease the cell size until the difference in the results is not significant. To choose a proper grid resolution, FDS User's guide suggests calculating the non-dimensional expression:

$$\frac{D^*}{\delta x} \tag{3.1}$$

which should range between 4 and 16 according to the validation study sponsored by the U.S. Nuclear Regulatory Commission [39]. δx is a nominal size and D^* is a characteristic fire diameter:

$$D^* = \left(\frac{\dot{Q}}{\rho_\infty c_p T_\infty \sqrt{g}}\right)^{\frac{2}{5}} \tag{3.2}$$

Where:

- $\dot{Q}$ - the total heat release rate [kW/m^2];
- ρ_∞ - the air density (=1.2 kg/m^3);
- c_p - the air thermal capacity (=1.0 kJ/kgK);
- T_∞ - the ambient air temperature (= 293 K);
- g - the gravitational acceleration (=9.81 m/s^2).

The results for the characteristic fire diameter and the non-dimensional expression are presented in Table 6.

Table 6. The characteristic fire diameter and the non-dimensional expression

		Scenario 1		**Scenario 2**		**Scenario 3**	
Wind conditions		**No wind**	**Wind**	**No wind**	**Wind**	**No wind**	**Wind**
HRR [kW/m^2]		1920.0	2050.0	1920.0	2050.0	1920.0	2050.0
D* [m]		4.6	4.7	5.8	6.0	7.7	7.9
Mesh size [m]	**0.2**	23.0	23.5	29.0	30.0	38.5	39.5
	0.4	11.5	11.8	14.5	15.0	19.3	19.8
	0.8	5.8	5.9	7.3	7.5	9.6	9.9
	1.2	3.8	3.9	4.8	5.0	6.4	6.6

3.3.4 Sensitivity study

Accuracy of FDS models results in a long run time. High demands in terms of the computing time push designers to increase the grid size, often without taking into account the consequences that this could bring to the results. As example of a previous study, Petterson compared two sets of experiments with their numerical models created in FDS. These models were run for different grid sizes. The study was based on the McLeans Island tests performed in two isorooms, each 2.4 m x 3.6 m x 2.4 m with the heat release rate equal to 55 kW and 110 kW. The second set of experiments was conducted in the US Navy Hanger in Hawaii. Large-scale tests were performed in the 98 m long, 74 m wide and 15 m high hangar. The used heat release rates were 5580 kW and 6670 kW, respectively [20].

The results showed that there is no rule that one grid size gives better results than the other. It is usually expected that finer grid gives more accurate results. However, it was not always the case. Coarse grid sizes can lead to cancelling each other out conflicting errors and better predictions are made. Another reason that has to be taken into account, is that experiments data have also some inaccuracy. To make a comparison between numerical model and tests results, the level of imprecision should be assessed for the latter one. It can be done by comparing obtained data with available analytical methods. Nevertheless, all FDS models predicted much better the experimental temperatures for the points located out of the plume, where there is a less turbulence [20].

Finite number of studies has been performed on the effect of using different grid sizes. The available data show that smaller grid gives better results of the temperature in the plume along the centreline of a flame. However, the Hawaii hanger tests showed that the temperature predictions for all used grid sizes were not accurate. It is explained that the grid size was still too big to solve properly all the small scale eddies and turbulence phenomena [20]. Davis et al (1996) noticed that the grid of one tenth of the fire diameter gives relatively accurate results for the plume centreline temperatures. It means that for the considered scenario the grid size should be maximum 1.1 m [40].

In this thesis, in order to get the results which are the most independent of the grid size, the sensitivity study is performed for Scenario 4B assuming following grid cell sizes: 120 cm, 80 cm, 40 cm and 20/40 cm. In the last case, the grid size is 20 cm within the domain where the points of interest (staircase, some beams and columns, temporary compartment, muster area, fire area) are localised and in their immediate surroundings. In the remaining area mesh is 40 cm (Table 7).

Table 7. Grid size and corresponding number of elements within the computational domain

Grid size [m]	Number of elements
1.2	12 960
0.8	43 740
0.4	349 920
0.2/0.4	1 522 894

Figure 19 shows the heat release rate diagram over the time. The results are not surprising since the same constant HRRPUA is assigned to each model and considering the fire are equal to 94.7 m^2 and the HRRPUA = 2050 kW/m^2, the total HRR should be 194.4 MW.

To choose the model for further study with the grid resolution that gives the most reliable predictions, the temperatures and radiative heat fluxes are compared for the points at different distances in the east direction from the fire area. Figure 20 present the results for the temperature development while Figure 21 presents the results for the radiative heat fluxes at the height of 1.5 m from the cellar deck.

It would seem that Figure 20 shows too low temperature predictions for the point above the fire for models with the grid size of 40 cm and 20/40 cm. The averaged temperature is 82 °C and 45 °C, respectively. For model with 20/40 cm grid size, as well as 40 cm grid size, the height of the flame just above the fire area, is much lower compare with 80 cm and 120 cm grid resolution, what is shown in Figure 22. The flame is tilted and dragged due to the wind and most of the time does not affect that much the point where the temperature was measured. For 20/40 cm and 40 cm grid size models, the continuous flame is observed to be below the height of 1.5 m from the fire base, contrary to the models with bigger grid size where the height of the continuous flame exceeds 1.5 m. Additionally, there is a continuous supply of air at ambient temperature which decreases the temperature, so the results could be reasonable.

For the distance 5.8 m from the fire, models with 80 cm and 120 cm still give higher temperature predictions, the reason for that can be the same as for the point just above the fire area since it is also effected by the flame. For the distances 12.4 m and 19.0 m, the relation is reversed – models with finer resolution predict higher temperature. The results for these models are considered to be more reliable according to the general rule that smaller grid size gives more accurate results.

A large discrepancy is observed for the radiative heat flux in the areas close to the fire. Similar to Petterson study it is observed that in the larger distances from the fire plume the predictions are relatively independent on the grid resolution.

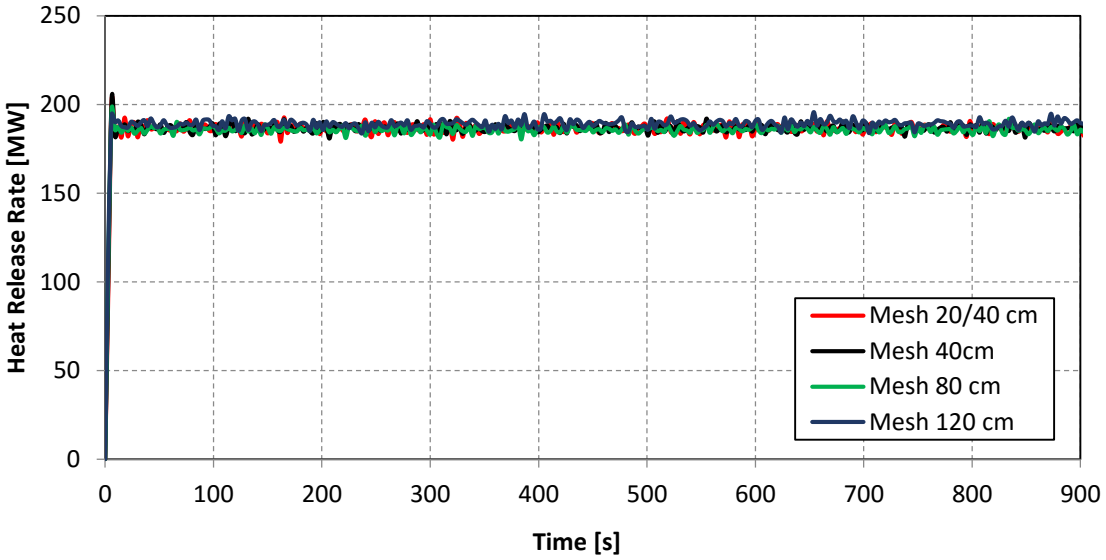

Figure 19. HRR for models with different grid resolution - Scenario 4B

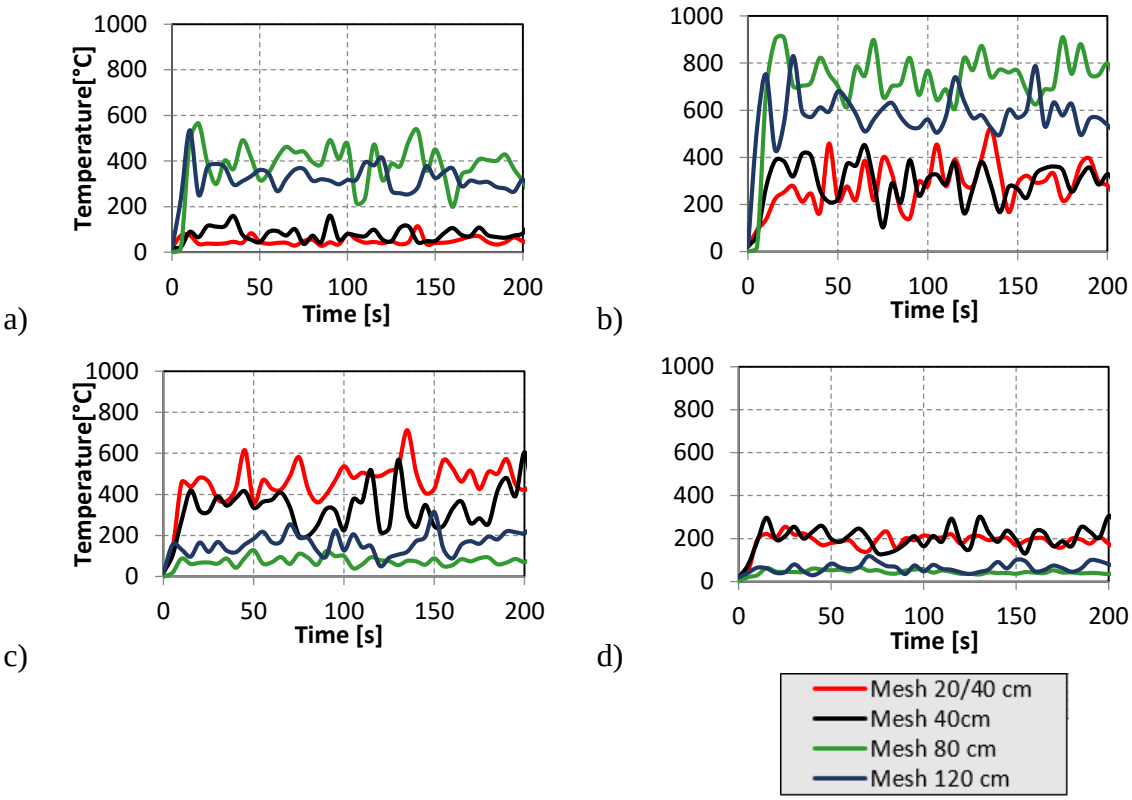

Figure 20. Temperatures for Scenario 4B at distances: a) 0 m, b) 5.8 m, c) 12.4 m, d) 19.0 m, from the fire centre

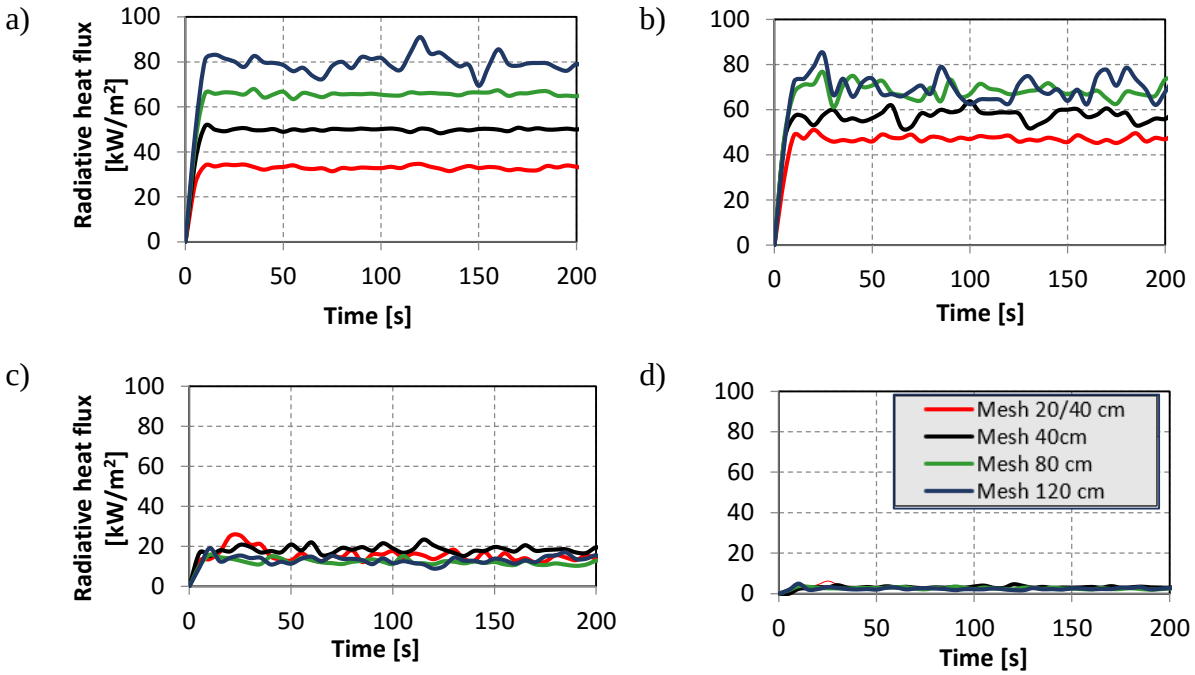

Figure 21. Radiative heat flux for Scenario 4B at distances: a) 0 m, b) 5.8 m, c) 12.4 m, d) 19.0 m, from the fire centre

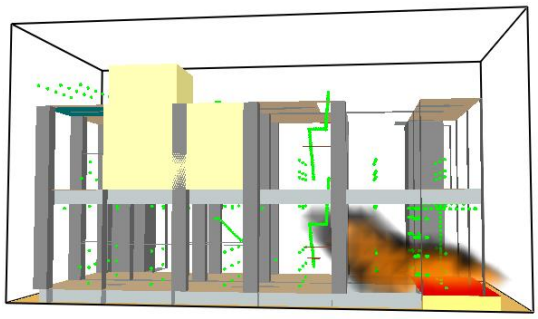

a) Mesh 120 cm

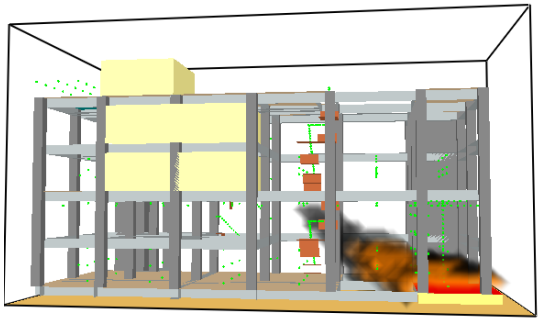

b) Mesh 80 cm

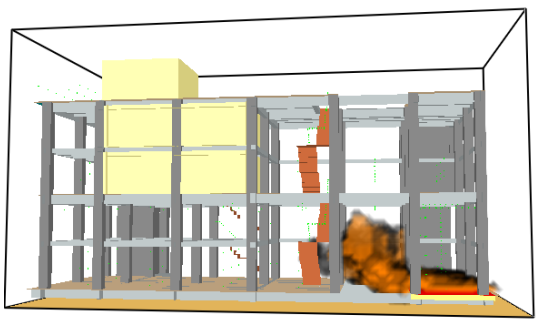

c) Mesh 40 cm

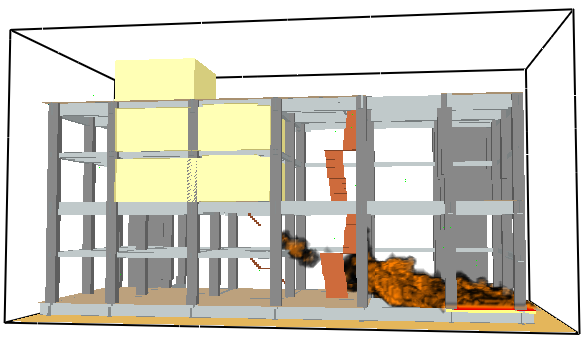

d) Mesh 20/40 cm

Figure 22. Flame at 30 s for different grid sizes – Scenario 4B

3.3.5 Run times

As it was remarked before, FDS software is extremely demanding in terms of process time and amount of RAM and this is mostly due to the size of the computational domain and the number of elements. Finer grid size leads to smaller time step size, so the number of iterations per time step is smaller. However, it increases the total number of iterations due to the larger number of time steps, so the computing time is larger.

Models with the full domain and fine grid sizes were the most problematic to run – Scenario 3 and Scenario 4. Models with 20/40 cm grid resolution and full domain were possible to run only in a cluster after dividing the computational domain into 20 separate meshes, so each of them was assigned to own process. Models with 40 cm grid size were run on 16 GB computer and the computational domain did not need to be necessarily divided into more meshes. Models with 80 cm and 120 cm grid resolution were relatively fast to run on 8 GB computer. Fortunately, the analysis could be run only to obtain 200 s of simulation because steady-state was reached after 10 s of simulation and it was enough for radiative heat flux study.

It took less time to run models for Scenario 1 and Scenario 2 which apply to the reduced domain – around 20 % of the full domain volume. It enabled to decrease the grid size even to 10 cm for some models.

In case of Scenario 3 and Scenario 4, considering the run time and accuracy, models with 40 cm grid size seem to be the most appropriate. For Scenario 1 and Scenario 2 models with 10 cm grid sizes give the closest results to the analytical methods. Table 8 presents random scenarios and the time and memory that they required.

Table 8. FDS models running times

Scenario	Mesh size	Computer capacity	Simulation time	CPU time
1	10 cm	cluster	450 s	170.7 hr
2	10 cm	cluster	200 s	96.4 hr
3A	20/40 cm	cluster	900 s	76.6 hr
3A	40 cm	16 GB	900 s	29.5 hr
3A	80 cm	8 GB	900 s	2.9 hr
3A	120 cm	8GB	900 s	1.2 hr
4A	20/40 cm	cluster	200 s	73.4 hr
4A	40 cm	16 GB	200 s	7.0 hr
4A	80 cm	16 GB	200 s	0.5 hr
4A	120 cm	8 GB	200 s	0.2 hr
4B	20/40 cm	cluster	900 s	185.0 hr

4. COMPARISON OF THE ANALYTICAL AND NUMERICAL MODELS

4.1 Localised fires

Scenario 1 and Scenario 2 are verified using the expressions given in Eurocode **[10]** for localized fires as it was presented in section 2.3. In case of Scenario 1, the flame is not impacting the ceiling so the Heskestad approach is applied. The fire in Scenario 2 qualifies for Hasemi method (Table 9). Both scenarios are run in the reduced computational domain (14.8 m x 22.8 m x 15.2 m). Before that, a short study was done to check if reducing the domain influences the output data. This study is presented in 4.1.2.

Table 9. Selection of the validation method

Scenario	The effective fire diameter, D [m]	The heat release rate, $\dot{Q}$ [MW]	The flame height, L_f [m]	Method for validation
Scenario 1	2.3	7.7	6.1 < 8.0	Heskestad
Scenario 2	5.7	49.2	11.8 > 8.0	Hasemi

4.1.1 Heskestad model

Heskestad model allows to determine the temperature in the plume along the vertical flame axis. However, it is important to specify what in this case means the plume.

In fact a fire plume is composed of three basic regions [47]. Near the bottom where the fuel burns there is a continuous flame (red colour in Figure 23 indicates the flame). Above this there is an inherent flame region. In this area flame may or may not exist due to the pulsing and entrainment. Above this region there is buoyant plume where the physical flame does not exist but still it is considered to be the fire plume because hot gases rise due to buoyancy. This region is indicated by green colour above the flame in Figure 23 and Heskestad's expression is valid exactly for this area.

The estimation of the flame height in FDS can be done by analysing the simulation in Smokeview and counting the number of cells in the vertical direction which are occupied by

the flame half of the time. Sticking with this approach, a rough estimation gives the flame of 7.0 m high.

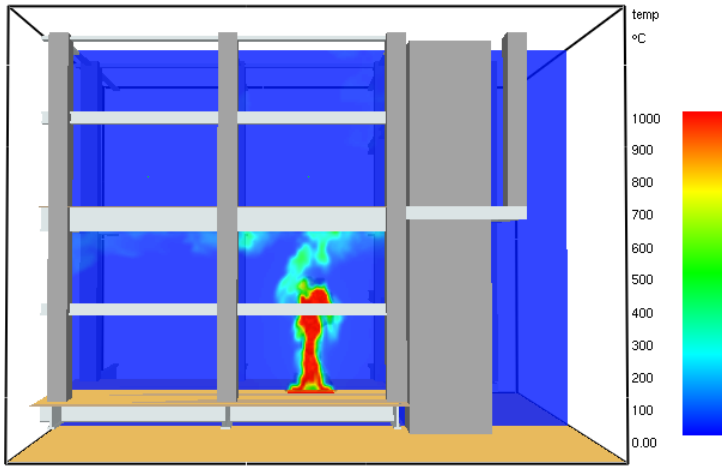

Figure 23. Fire plume – Scenario 1, mesh 10 cm

Figure 24 presents the results for plume centreline temperatures according to Heskestad and output from FDS for 10 cm, 20 cm and 40 cm grid sizes. However, the convective part of the rate of heat release is taken as 0.7 $\dot{Q}$ instead of 0.8 $\dot{Q}$ for Heskestad's expression. This ratio corresponds to the value from the FDS analysis.

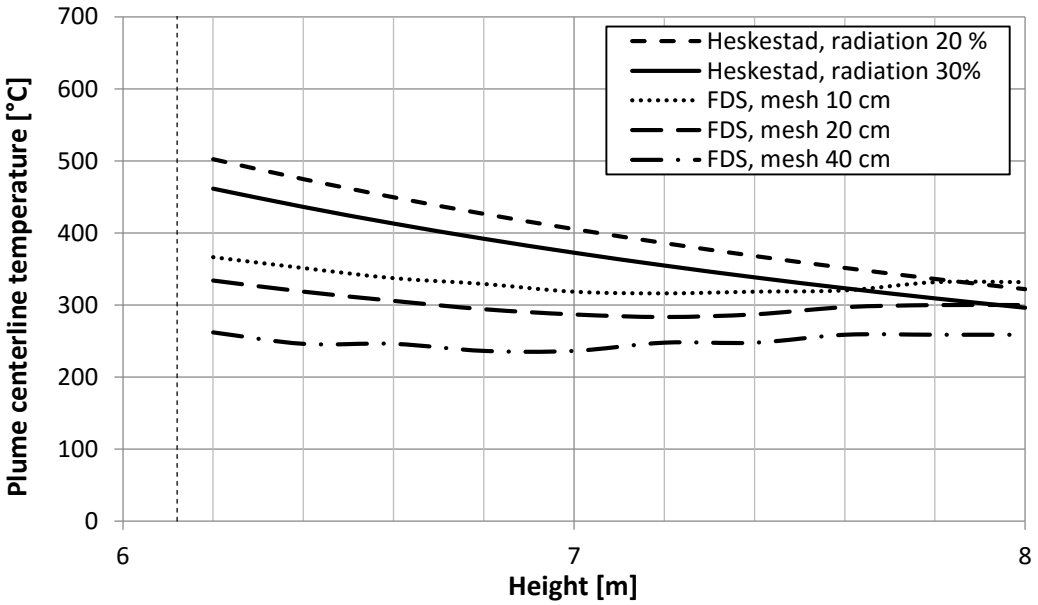

Figure 24. Plume centreline temperatures

Table 10 gives the deviation of the output from respective FDS models with respect to the Heskestad results with considering 30% of the heat transfer by radiation. The maximum

deviation from Heskestad's approach is 44 % for 40 cm grid resolution, 28 % for the FDS model with 20 cm grid resolution and 21 % for the FDS model with 10 cm grid resolution. Smaller grid size gives closer results to the analytical method. However, the most significant difference is just above the flame. The determined temperatures start to converge with the distance from the fire. It has to be highlighted that there is a secondary beam in the FDS model at the height of 7.5 m and the thermocouples are placed next to it. This can cause some inaccuracy in the numerical results.

Table 10. Divergence of the numerical results with respect to the Heskestad's results

Height	Heskestad	Mesh 10 cm		Mesh 20 cm		Mesh 40 cm	
[m]	[°C]	[°C]	%	[°C]	%	[°C]	%
6.2	461	366	-21	334	-28	262	-43
6.4	436	351	-19	319	-27	246	-44
6.6	413	337	-18	306	-26	246	-40
6.8	392	329	-16	294	-25	236	-40
7.0	373	318	-15	287	-23	236	-37
7.2	355	316	-11	283	-20	248	-30
7.4	338	318	-6	287	-15	248	-27
7.6	323	320	-1	297	-8	259	-20
7.8	309	332	7	300	-3	259	-16
8.0	296	332	12	300	1	259	-13

4.1.2 Hasemi model

This method allows calculate the heat flux received by the surface area at the ceiling level. In FDS model the heat flux is measured at points which are presented in Figure 25. They are localised on the bottom flange of the beams.

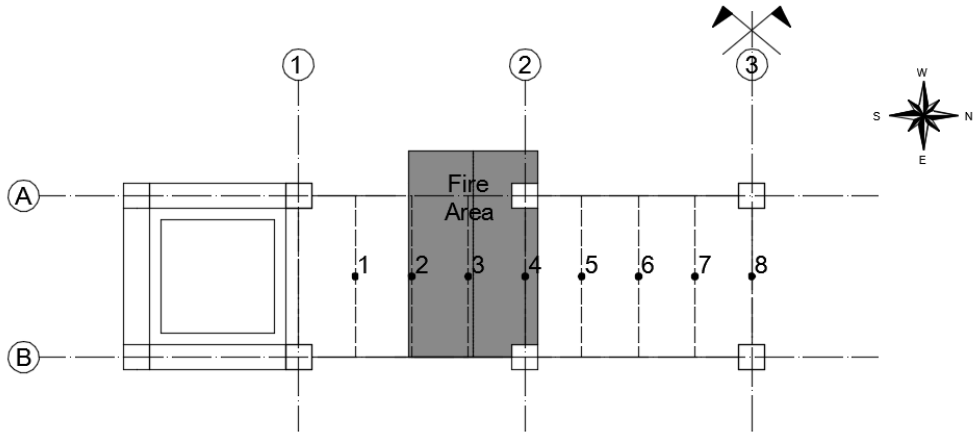

Figure 25. Localisation of the gauges in FDS models

As it was mentioned before, FDS results are highly sensitive to the grid size. However, due to the computer capacity and the run time it was impossible to run the model with the grid resolution bigger than 20 cm for the full domain. From this reason, the domain is decreased, since the results in the vicinity of the fire are needed. It was expected that reducing the domain will not significantly impact results. However, to prove this assumption two models were run both with 20/40 cm grid sizes, the difference was only in the size of the computational domain. The obtained heat flux for points 5-9 brought the desired output, as it is presented in Figure 26. This study proved that Scenario 1 and Scenario 2 may be run in the reduced computational domain.

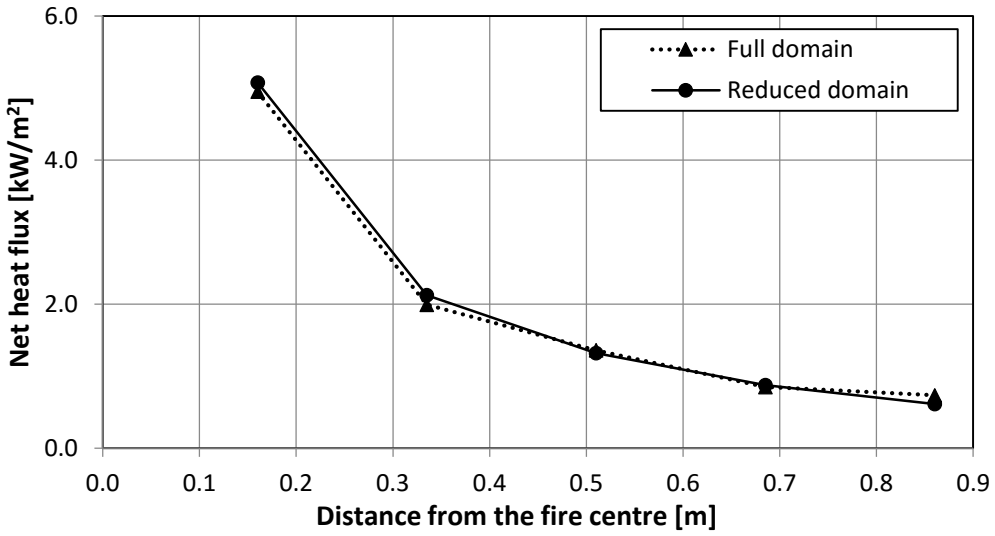

Figure 26. Results due to the domain size

The maximum net heat flux received by the points 1-8 is presented in Figure 27. The analytical calculations consider the configuration factors. As can be seen, the closer to the fire the values from model with 20 cm grid resolution are more over predicted if compared to the analytical results. Model with 10 cm grid size gives much closer estimations however it seems that it underpredicts the heat flux received by the surface. According to Eurocode the upper deck is impacted by the flame since its height was calculated as 11.8 m. However, FDS simulation does not show this same behaviour. In the numerical models the flame only from time to time impacts the ceiling so probably Hasemi's model gives higher results to keep the safety margin. All models evaluate similar results with the distance from the fire. Table 11 presents the divergence of the numerical results with respect to analytical. It would be useful to run at least one more model with for example 15 cm grid size to see better the trend due to the grid resolution. Figure 28 shows a hot layer of gases which accumulate under the deck.

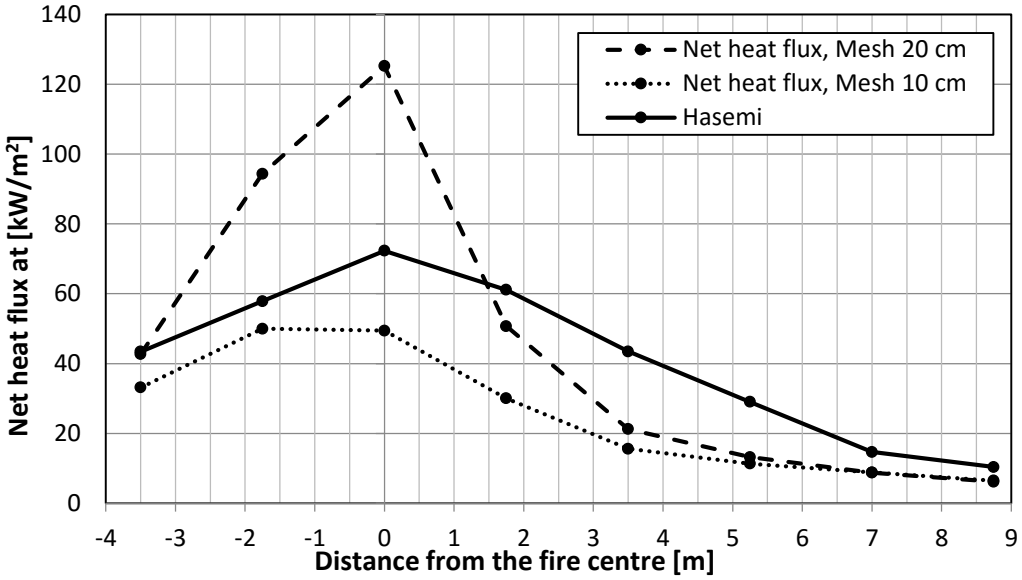

Figure 27. The net heat flux received by the beams – Scenario 2

Table 11. Divergence of the numerical results with respect to the Hasemi's results

Gauge number	Hasemi	Mesh 10 cm		Mesh 20 cm	
	[kW/m²]	[kW/m²]	%	[kW/m²]	%
1	43	33	-24	43	-2
2	58	50	-14	94	63
3	72	49	-32	125	73
4	61	30	-51	51	-17
5	43	16	-64	21	-51
6	29	11	-61	13	-55
7	15	9	-40	9	-40
8	10	6	-38	6	-41

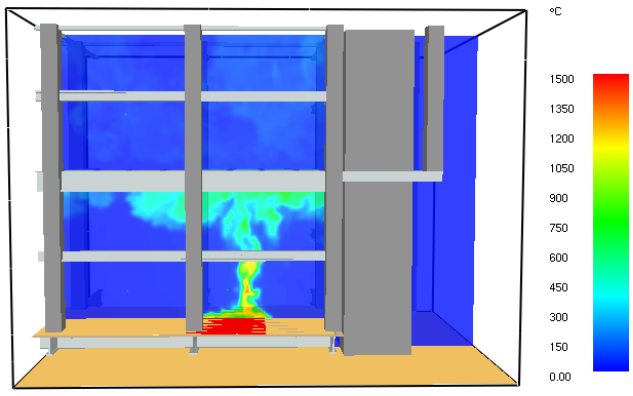

Figure 28. Temperature distribution in the fire plume after 130 s – Scenario 2

Table 12 shows the distribution of the heat transfer for points 1-8. As can be seen, the heat transfer is mostly by radiation what is more highlighted closer to the fire. For the beam just above the fire, the radiative heat flux makes up 90 % of the net heat flux.

Table 12. Distribution of the heat transfer

Point	1	2	3	4	5	6	7	8
Convection	20%	12%	10%	20%	25%	38%	41%	58%
Radiation	80%	88%	90%	80%	75%	62%	59%	42%

4.1.3 Final remarks

• For localised fires not impacting the upper deck, FDS models with finer resolution predict higher temperatures in the plume along its centreline what reflects better the results obtained from Heskestad's expression presented in Eurocode [10]. The difference between numerical and analytical results decreases with the distance from the fire flame.

• Model with 10 cm grid size gives relatively close output to the results based on the methodology given in Eurocode for localised fires not impacting the upper deck [10].

4.2 The radiative heat flux for large pool fires

The analytical models for the radiative heat flux predictions presented in 2.4 are used to verify the numerical model. However, it has to be kept in mind that the most reliable validation should be done by comparison with the experiments. Unfortunately, no experimental tests were done in favour of this case study. In this section the comparison is focused on Scenario 3 and Scenario 4.

4.2.1 Heat fluxes in FDS

Before starting to examine the results from FDS, it is important to explain the various heat flux quantities that this software provides us with. Namely, there are following options [48]:

- RADIATIVE HEAT FLUX - $\dot{q}''_{rad}$
- CONVECTIVE HEAT FLUX - $\dot{q}''_{conv}$
- NET HEAT FLUX - $\dot{q}''_{net}$
- INCIDENT HEAT FLUX - $\dot{q}''_{inc}$
- GAUGE HEAT FLUX - $\dot{q}''_{gauge}$
- RADIOMETER - $\dot{q}''_{radiometer}$

- RADIATIVE HEAT FLUX GAS - $\dot{q}''_{rad}$

Three first are used to obtain the heat flux to a surface that accounts for incoming (absorbed), outgoing (reflected) and convective heat transfer taking into account the actual temperature of the surface. It is important to highlight that the radiative heat flux considers an energy balance on a surface (it is reduced by the reflected heat flux):

$$\dot{q}''_{rad} = \dot{q}''_{rad,in} - \dot{q}''_{rad,out} \tag{4.1}$$

$$\dot{q}''_{conv} = \alpha_c (T_g - T_w) \tag{4.2}$$

$$\dot{q}''_{net} = \dot{q}''_{rad} + \dot{q}''_{conv} \tag{4.3}$$

Where:

$$\dot{q}''_{rad,out} = \dot{q}''_{rad,in} - \varepsilon\sigma T_w^4 \tag{4.4}$$

while T_g and T_w are the local gas temperature and the surface temperature, respectively. The GAUGE HEAT FLUX also accounts for the incoming and outgoing radiation and convection and additionally adjusts the heat fluxes according to the surface temperature:

$$\dot{q}''_{gauge} = \dot{q}''_{rad,in}/\varepsilon_m + \dot{q}''_{conv} + \sigma(T_w^4 - T_G^4) + \alpha_c (T_w - T_G) \tag{4.5}$$

T_G is the gauge temperature. The same refers to the RADIOMETER output quantity except the fact that convection is neglected. Both GAUGE HEAT FLUX and RADIOMETER quantities should be used when experimental measurements are compared.

In case of INCIDENT HEAT FLUX, only incoming radiation and convection are considered and this output is mainly used for a diagnostic (radiative losses are neglected). The RADIATIVE HEAT FLUX GAS quantity corresponds the radiative heat flux, except that this device does not have to be placed on a solid surface in FDS software.

To have the feeling what is the difference between them, Figure 32 presents the comparison between different heat fluxes (except the gauge heat flux, which requires the gauge temperature to be specified). This study was done for Scenario 3A at the distance of 6 m from the centre of the fire and 40 cm grid size.

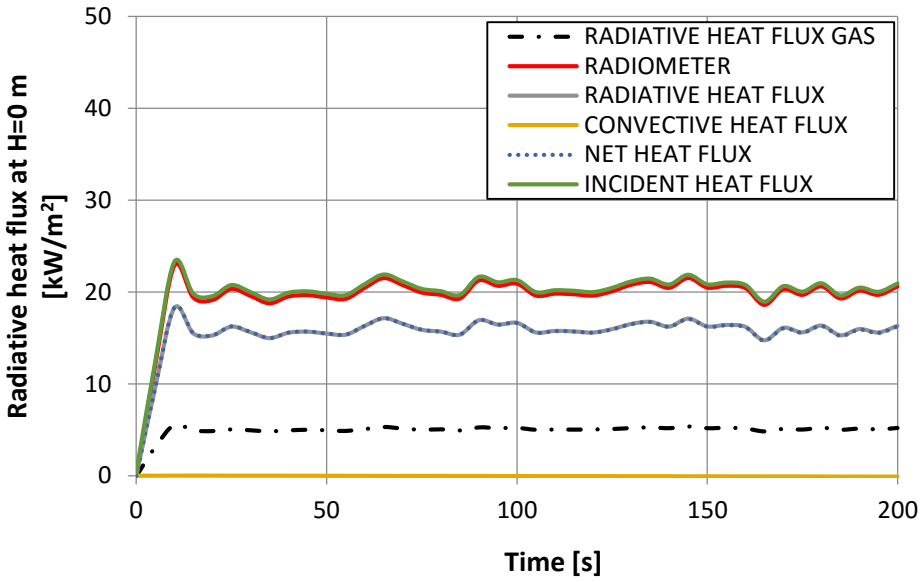

Figure 32. Comparison of heat fluxes in FDS

The incident heat flux and radiometer heat flux are overlapping at around 20 kW/m^2. Due to the fact that the steel plate has an emissivity 0.8, the radiative heat flux is lower – it oscillates around 16 kW/m^2 (20% of radiation is reflected away). As the steel plate heats up, it starts to transfer heat outwards by convection, hence the negative convective heat flux of approximate -0.09 kW/m^2. Since this value is very small, the difference between the radiative and the net heat flux cannot be seen. The same concerns the incident heat flux which overlaps the radiometer heat flux due to the small convection.

According to Overholt [48] radiative, convective and net heat fluxes should be used when the heat flux to a "hot" target is evaluated and the actual surface temperature is considered. The conservative approach, used for many hazard calculations, evaluates the heat flux to a "cold" targets by using gauge or radiometer heat flux. However, because the analytical methods do not require the specification of the surface emissivity, the most reasonable is to compare the data from analytical methods with the RADIOMETER quantities.

4.2.2 Verification of the points of interest

In the numerical model, the gauges to measure the heat flux are placed as it is shown in Figure 29. The devices are localized on the deck plate, at the same level as the fire area. For the radiative heat flux determined by FDS it is observed that after 10 s the steady-state is reached. From this reason the data are reduced by averaging them excluding first 10 s.

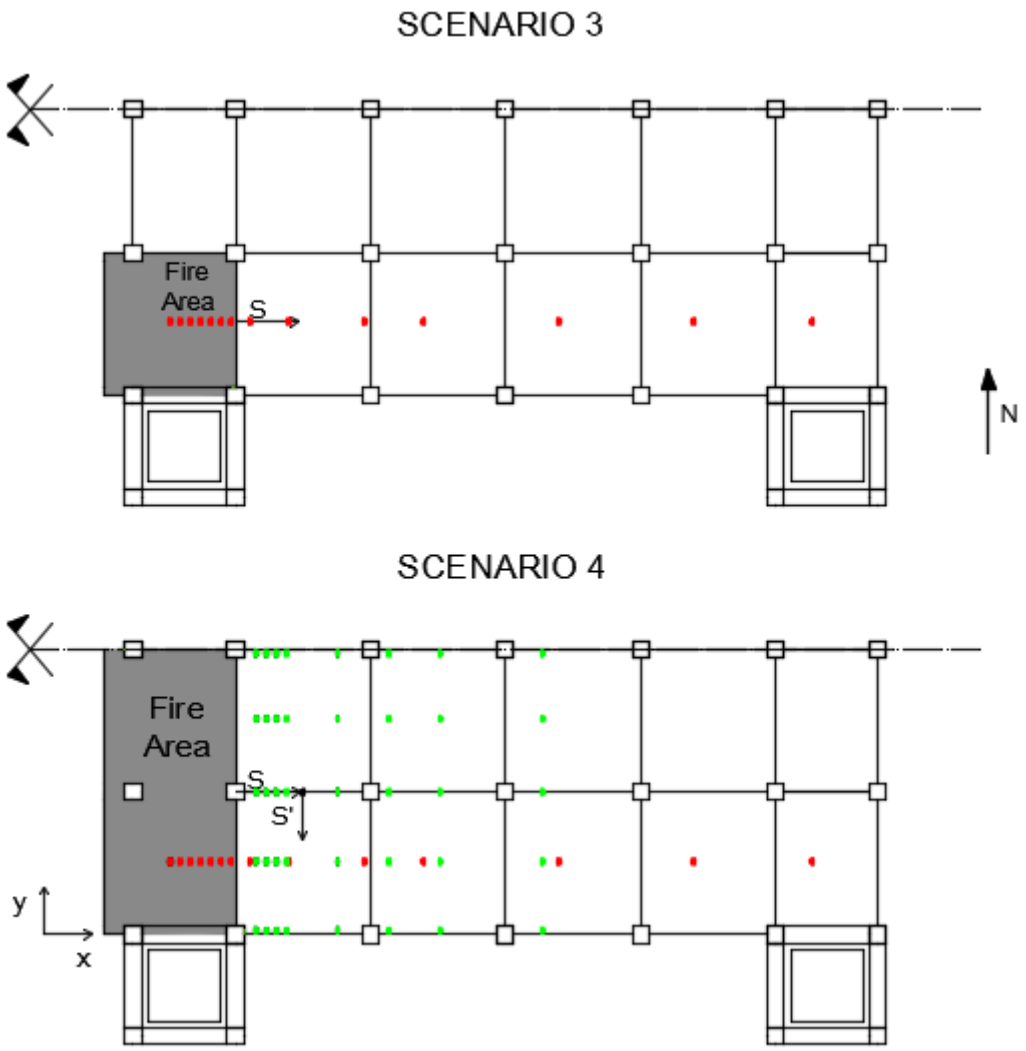

Figure 29. Points of interest for the radiative heat flux comparison

The analytical methods do not account for the radiation emitted from the elements. Moreover, they are limited in terms of considering the impact of the obstacles, like columns in the studied case. It means that in case of Scenario 4 the heat flux calculated at the distances S from the fire area would give even higher predictions if compared to points at the distance S' from the centreline. This fact makes a relevant difference between the analytical and numerical models, in favour of the latter one where the results are space dependent.

In the numerical model first, the data measured in green points are analysed (Figure 29). As presented in Figure 30, the shadow from the columns contributes towards lower values of radiative heat fluxes along the centreline. Figure 31 presents the localizations of these gauges in FDS model (also green points).

Due to the higher radiative heat fluxes in between columns (along y) the results from red points are taken for the radiative models comparisons what is described in the next sections.

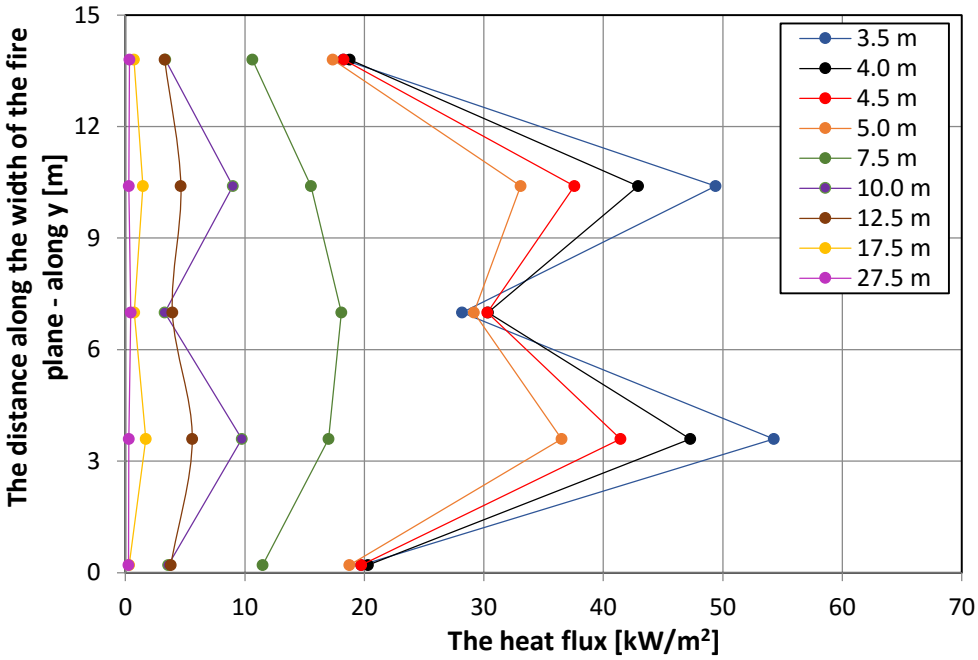

Figure 30. The variation in the FDS results due to the shadow effect from columns

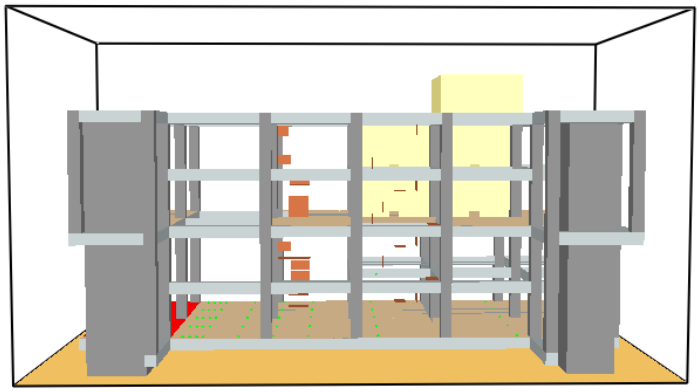

Figure 31. The localization of the gauges in the FDS model (green points)

4.2.3 Impact of the grid resolution on the results

Despite the sensitivity study in 3.3.3, Figures 33 and 34 show the radiative heat flux predictions for different grid resolutions. As it was mentioned by Davis and his co-authors, the grid of one tenth of the fire diameter gives relatively accurate results for the plume centreline temperatures [40]. It means that the grid sizes for Scenario 3A and Scenario 4A should not exceed 78 cm and 110 cm, respectively. It seems that the same limitation concerns the radiative heat flux predictions. As it can be seen from Figures 33 and 34, only in case of Scenario 3A, there is some sort of instability associated with the 120 cm grid size model because of a significant over prediction compare to other models in the flame region. All considered models for Scenario 4A give relatively similar results.

The results from models with 80 cm and 120 cm grid sizes display the constant radiative heat flux within some distances. This is associated with the fact that FDS numerically solves the equations for each cell. It means that one value corresponds to one grid element. The values from FDS are taken each 50 cm, so some of them are overlapping on the diagram if the grid size is bigger than 50 cm.

Considering the CPU, model with 40 cm grid size is taken as the representative for further study.

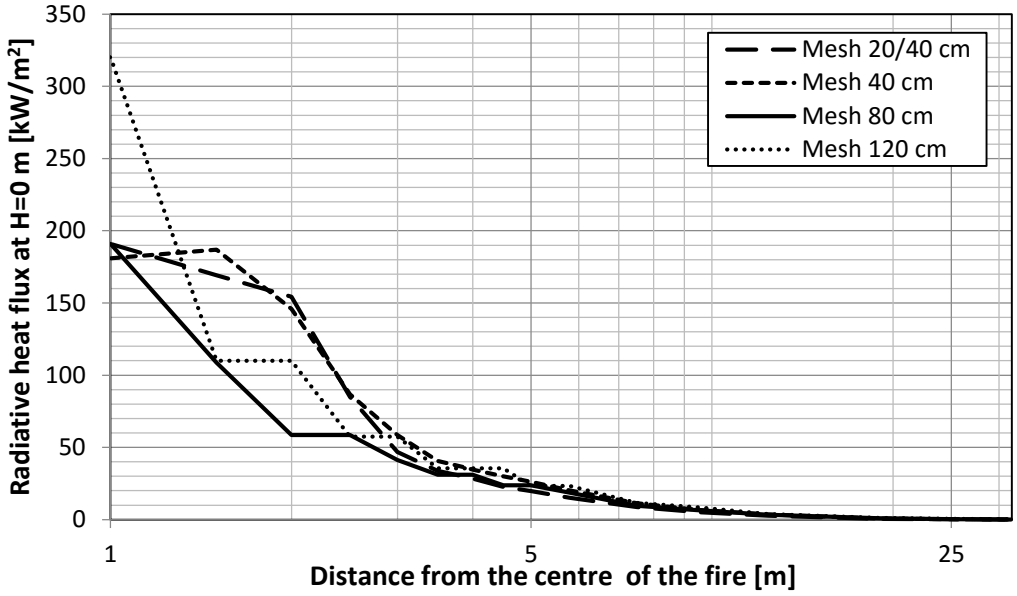

Figure 33. Radiative heat flux due to the distance from the fire centre – Scenario 3A

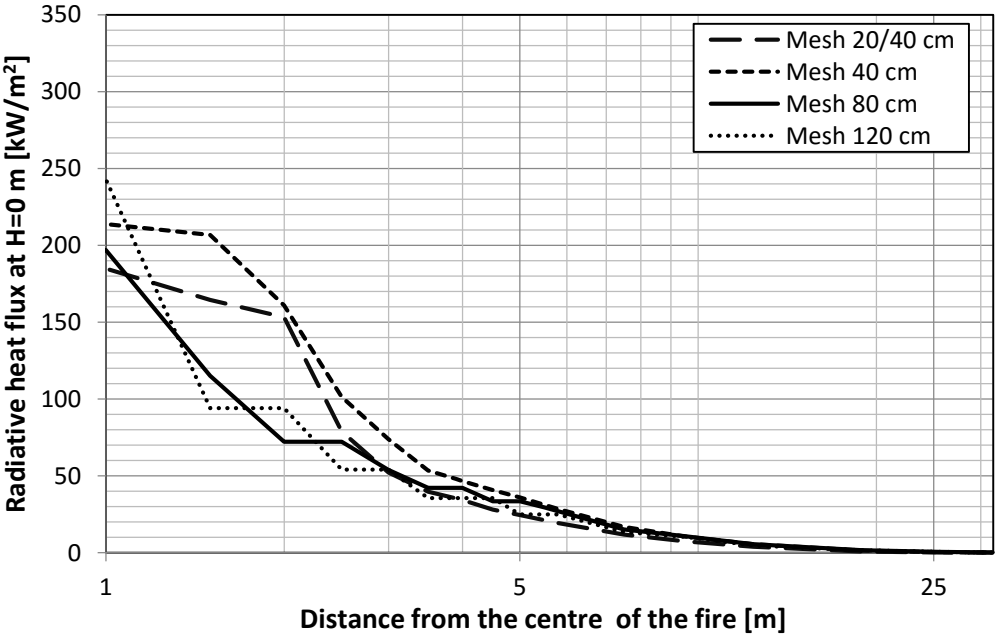

Figure 34. Radiative heat flux due to the distance from the fire centre – Scenario 4A

4.2.4 Overview of model results

Before reviewing each model individually, it is useful to depict all models at one diagram to get a feel for the difference between them. Figures 35 and 36 show the change in the radiative heat flux with the distance away from the fire centre. For analytical models it is possible only to calculate the heat flux outside the flame which for the models based on solid flame assumption is a cylinder in shape with specified diameter. Hence, the plots start from 3.9 m for Scenario 3A and from 5.5 m for Scenario 4A.

As can be seen, the FDS output data are within the analytical models predictions. However, it is noticeable that there is a relatively significant range of values predicted by considered radiation models. Some remarks will be addressed to all presented methods in order to find reasonable explanation for such a divergence.

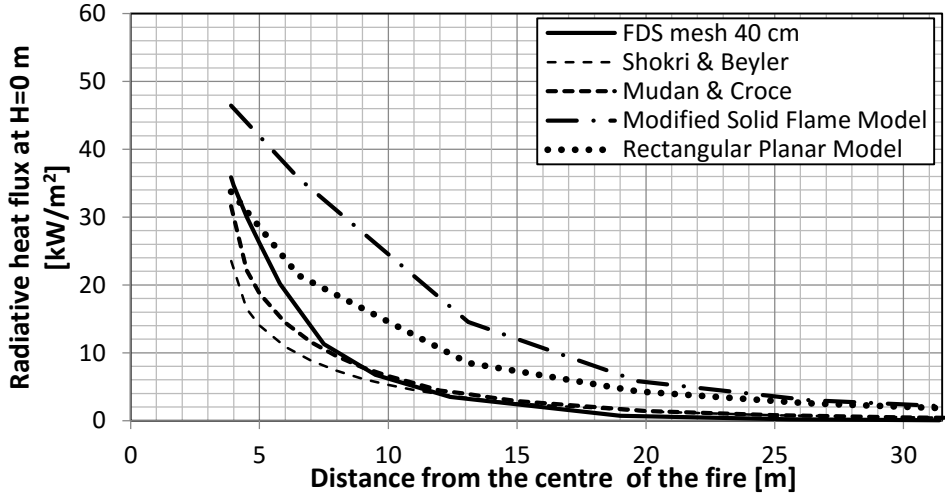

Figure 35. Comparison of the models – Scenario 3A

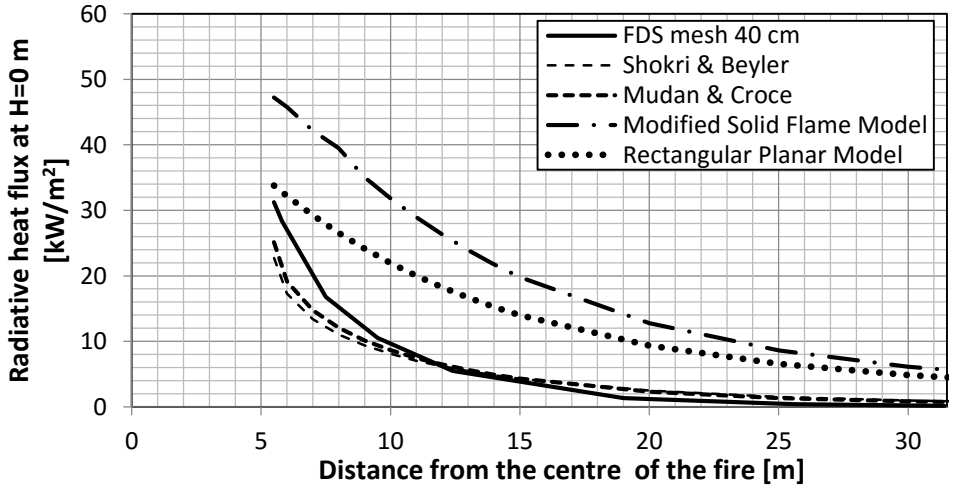

Figure 36. Comparison of the models – Scenario 4A

4.2.5 Solid Flame Models assumptions

First, three analytical models are compared each other. It has to be stressed that the Rectangular Planar model is in this study based on the Modified Solid Flame model. The difference is embedded in the defining the configuration factors. The comparison between those two methods will be done separately.

All three correlations: Shokri & Beyler, Mudan & Croce and Modified Solid Flame model are based on the same common assumption that the flame is cylindrical in shape and emits the thermal radiation from its sides. However, both Shokri & Beyler and Mudan & Croce methods employ the emissive power averaged over the flame height of the fire [35]. The threshold value for the average emissive power which is used by HUD to define the Acceptable Separation Distance for buildings is 31.5 kW/m^2 [36]. Both methods fall under this limit for fires bigger than 30 m in diameter (Figure 37). This could be wrongly interpreted that the building can be localised just next to the sites with likely to occur pool fires because the predicted radiative heat flux would be never grated than 31.5 kW/m^2.

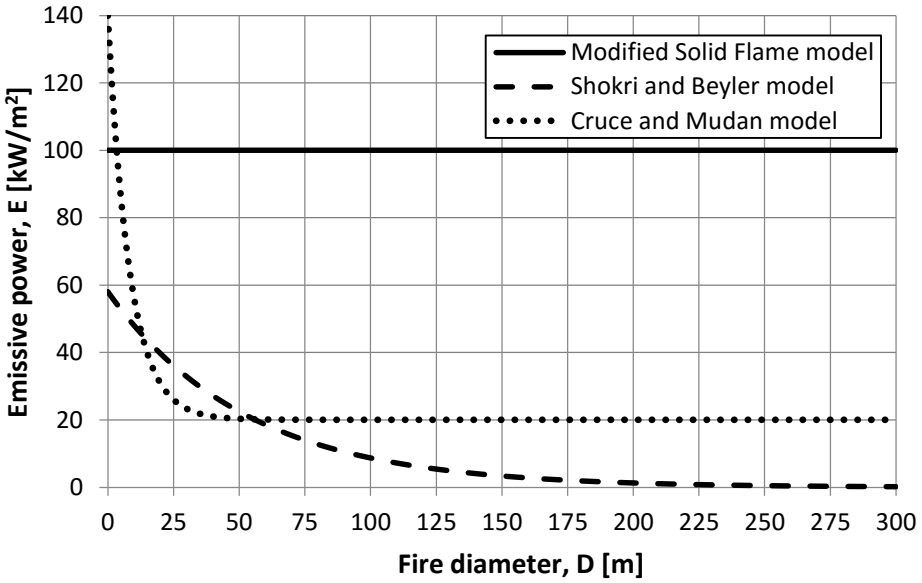

Figure 37. Emissive power as a function of fire diameter for a crude oil pool fire

To bypass the problem that nearby the fire the emissive power was under-predicted, the Modified Flame Model was introduced. This approach takes constant emissive power equal 100 kW/m^2. In this approach, the flame height refers only to the luminous flame zone, as it is explained in detail in 2.4.3. As opposed to Shokri & Beyler and Mudan & Croce models, the Modified Flame Model may over predict the results. It has been highlighted by NIST that for the near-field calculations and assumption of 100 kW/m^2, the results are conservative since this method is intended to yield cautious estimates of Acceptable Separation Distance. This explains

the fact that Modified Flame Model gives the highest radiative heat flux among all considered approaches.

Referring once more to Figure 37, it can be seen that for fires 7.8 m (Scenario 3A) and 11.0 m (Scenario 4A) in diameter, Cruce and Mudan give higher prediction of the emissive power, if compared with Shokri and Beyler approach. This is consistent with Beyler findings that Cruce and Mudan assumption for the emissive power might be too conservative [49].

4.2.6 Comparison of the configuration factors from the Rectangular Planar Model and tabulated data form the Modified Solid Flame model

The configuration factors for both methods are presented in Figure 38. The deviation is embedded in defining the position of the radiating surface. The Rectangular Planar model assumes the radiating surface passing the centre of the fire flame. In contrast, in the Modified Solid Flame model the configuration factor is calculated for the leading edge of the fire. Exactly the same shape factors are determined from the rectangular planar model assuming the radiating plane crosses the leading edge of the fire. Modified Solid Flame model based on tabulated data might overestimate the configuration factor since it is never the case that the flame shape is perfectly cuboid and emits the radiation from its sides.

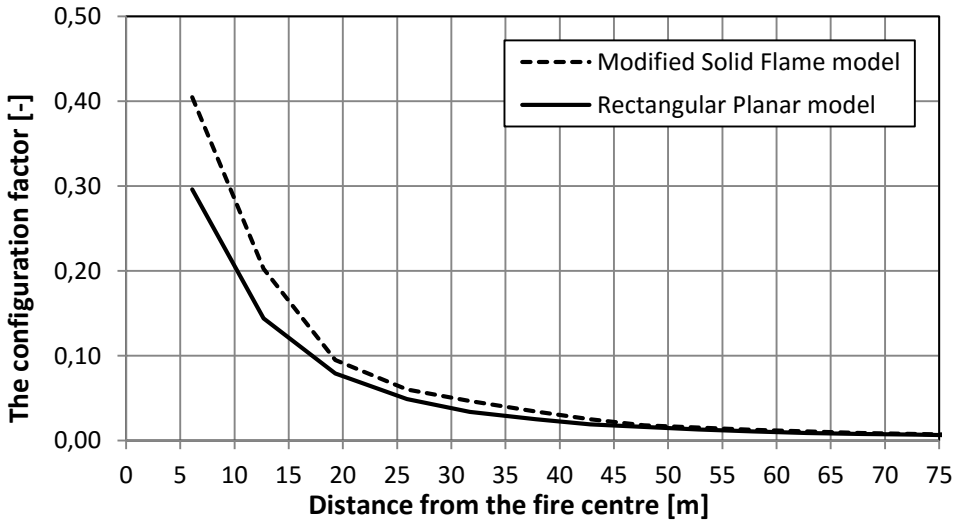

Figure 38. Comparison of the configuration factors

4.2.7 Flame height

The analytical methods are characterized by different way to determine the flame height. In case of Modified Solid Flame model, the flame height refers only to the luminous region. Figure 39 presents the radiative heat flux due to the height above the flame (at the distance 6.5 m from

the fire centre) for Scenario 3A. The maximum heights on the diagram indicate the flame height predicted by each method.

The predicted flame height is closely related to the value of the radiative heat flux. The higher flame height, the lower radiative heat flux at a particular distance from the deck, since the emissive power is assumed to be uniformly distributed over the flame height.

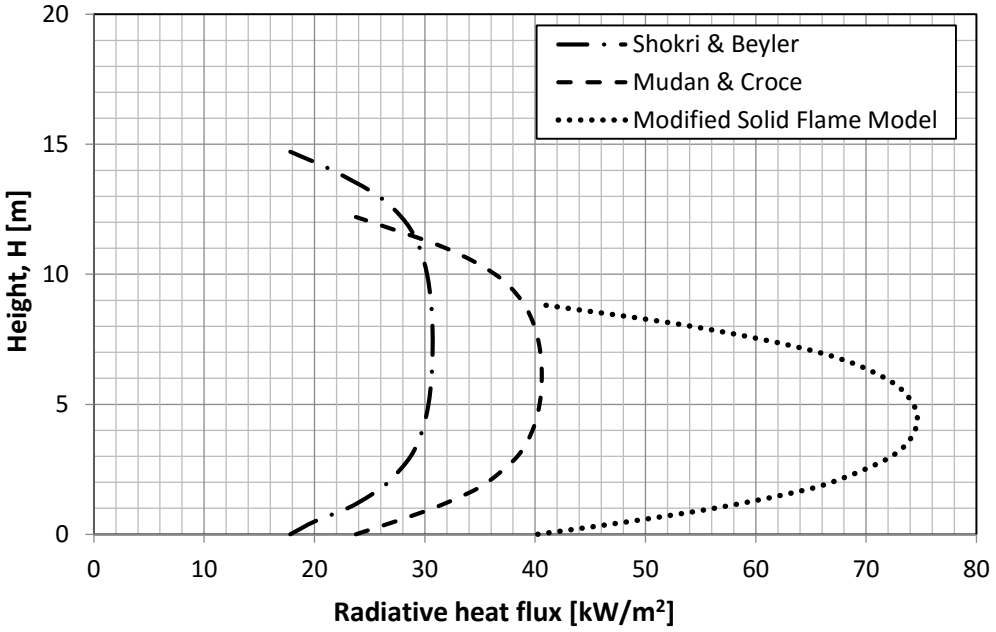

Figure 39. Radiative heat flux due to the height – Scenario 3A

The value of the heat flux varies with the height. The reason for this is due to the shape factors. Considering the solid flame model and the target at the ground level (which corresponds to the base of the fire), it receives large radiation from the bottom half of the cylinder however much less from the top half. When the target is located at height which corresponds to the mid-height of the cylinder, it receives a large amount of radiation from both – bottom and top half of the cylinder.

Referring to the FDS model, Annex A gives snap shots of the flame at successive times over 300 s period for different grid resolution for Scenario 4A. The unstable nature of the flame is shown, especially for the grid size 20/40 cm and 40 cm. The flame reaches the main deck above. The flame strikes the deck from one side or both sides every once in a while. This effect is only seen for smaller grid sizes. As in case of the localised fire presented in 4.1.1, a rough estimation of the flame height in FDS was done and the results are presented in Table 13. However, it is difficult to define the flame height for the wind conditions since the flame is tilted and dragged and very unstable.

Table 13. Flame height comparison

Method	Scenario 3	Scenario 4
FDS, mesh 20/40 cm	8.0 m	8.0 m
FDS, mesh 40 cm	8.0 m	8.0 m
FDS, mesh 80 cm	8.0 m	8.0 m
FDS, mesh 120 cm	7.0 m	7.0 m
Heskestad	14. 7 m	18.7 m
Thomson	12.2 m	15.5 m
Modified Solid Flame model	8.9 m	10.6 m

Table 13 shows a significant difference between the flame height obtained in FDS and analytical methods. In case of numerical models, the flame is limited by the upper main deck so it gives 8.0 m high flame, except the model with grid size 120 cm where most of the time the flame does not even impact the deck. The mesh size is probably too big since the flame is almost stable and it does not picture a turbulent fire. It is largely down to the fact that due to too big grid size the fire is not properly resolved and the flame mixture fraction underestimates the flame height. It is explained in more detail in [11].

4.2.8 Effect of the wind on the radiative heat flux predictions

Figure 40 presents the results for Scenario 3B in which the wind of 5 m/s is considered. Similar tendency is noticed for Scenario 4B. The variation in the results due to the grid resolution is described in detail in the sensitivity study. If FDS outcome is considered as reliable tool, it seems that Mudan and Croce model may under predict even 3 times the results for the near-by distances. Comparing the real shape of the flame from Figure 22 d) with the predicted in Figure 41, the latter one seems to be a significant simplification.

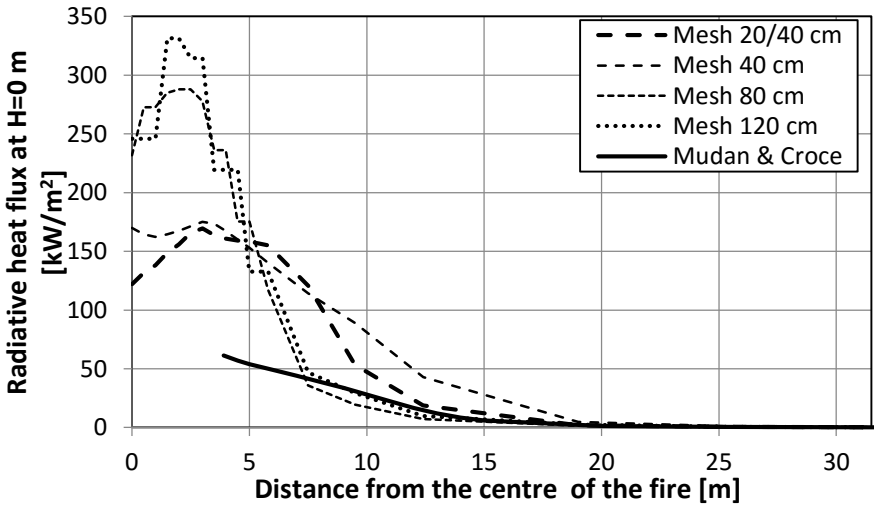

Figure 40. Radiative heat flux in wind conditions - Scenario 3B

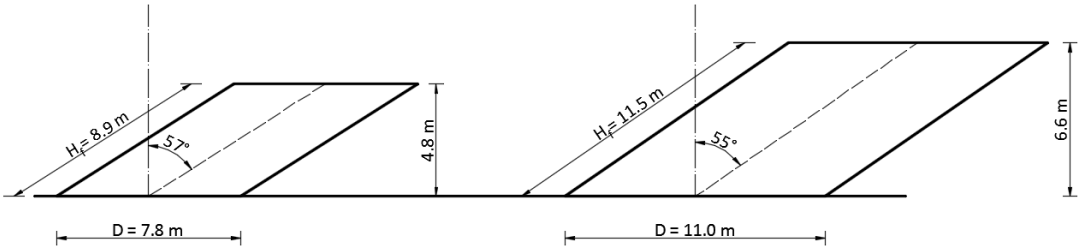

Figure 41. Predicted by Mudan and Croce the flame shapes: left-Scenario 3B, right – Scenario 4B

4.2.9 Final remarks

The study presented above is to verify the FDS analysis results for the radiative heat flux. The results from both Shokri and Beyler as well as Mudan and Cruce under estimate the radiative heat flux if compared to the FDS values. These models predict the realistic results, however, they are aimed to calculate safe separate distances between the fire and potential target and in that case safety factor of 2 is recommended [28] what leaves enough safety margins.

The analytical model that would consider the deck above the fire does not exist. This fact may bring some inaccuracy to the results and does not allow to compare the flame height from FDS analysis with the analytical results. In the analytical models the flame height was not reduced accordingly to the upper deck, this approach is assumed to be more reasonable. Otherwise, it could lead to underestimations because considered analytical methods take uniformly distributed emissive power over the fire height. Considering the full height may cause only a slightly higher predictions for the points localised on the fire level (due to the shape factors).

The speed of 5 m/s is relatively high value and significantly effects the flame shape. This might be the reason that Mudan and Croce model does not adequately predicts the radiative heat flux.

Separate study was done to examine the effect of the length-to-width ratio for the considered cylindrical solid flame models. Shokri & Bayler as well as Mudan & Croce models are valid when the mentioned ratio is around 1. No significant difference in over prediction or under prediction between those two scenarios is observed.

It is reasonable that the models alter in their predictions because of different assumptions that they are based on and also because of a wide range of fires that they can be applied to. Another aspect is related to inaccuracies in FDS which are mostly caused by the input variables specified in the software, as:

- the soot yield, which was taken as 2%. The soot fraction for crude oil varies between 1% and 2 % according to experiments [46]. Soot is in favour the radiative heat flux so the higher threshold was assumed for the safety reason.

- the radiative properties of species that can absorb and emit the thermal radiation and should be specified in FDS. Nevertheless, not all the fuels are tabulated. For absorbing species which are not known by the software, the FDS User's Guide recommends surrogate the fuel with the species with similar molecular functional group and molecular mass. In the studied case the default absorption data for methane are used. The influence of this modelling error on the final results is not assessed.

5. CONCLUSIONS AND FUTURE DEVELOPMENTS

5.1 Conclusions

• For localised fires not impacting the upper deck, FDS models with finer resolution predict higher temperatures in the plume along its centreline what reflects better the results obtained from Heskestad's expression presented in Eurocode [10].

• In case of localised fires impacting the upper deck, the net heat flux received by the fire exposed surfaces at the level of the ceiling, is dominated by radiation for elements close to the fire and decreases with the distance from the fire source in favour of the convective heat flux.

• The results for the temperature in the flame or next to it highly depend on the grid resolution. The same concerns the radiative heat flux however it was observed that all models with the grid sizes of maximum tenth of the fire diameter give similar results.

• In the further distances from the fire the predictions of the radiative heat fluxes are relatively independent on the grid size.

• The output for the radiative heat fluxes from the numerical models are within the predictions made by analytical methods. The difference is embedded in the assumptions that examined approaches are based on and probably in the input parameters used in numerical modelling.

• In case of Modified Solid Flame model, instead of the assumption that the radiating surface coincides with the leading edge of the fire and by moving this plane to the centre of the fire, gives closer values to the FDS estimations.

• For all studied numerical models the radiative part of the heat release rate oscillates around 30 %.

5.2 Future developments

• Presented FDS model requires the sensitivity study in terms of input data such as soot yield, HRRPUA, properties of the gases. The sensitivity study enables to observe which input parameters have the crucial impact on the output data. This is necessary to yield a sufficient conservatism in terms of both a personnel and a structure safety.

• An additional study would be appropriable to examine the effect of the wind for a wider range of wind velocities, starting from lower values. This would allow to analyse better the variation in the flame shape and its impact on the output data.

• As it was mentioned, for Hasemi model verification, it would be useful to run more models with different grid sizes to see better the trend for the net heat flux due to the grid resolution.

• The initial study was aimed to examine also the smoke migration and temperature development in terms of the safety of the personnel (Figure 42). From this reason staircases, temporary compartment and muster area are also included in the model. However, this requires to run more models for longer times to evaluate the visibility. Moreover, deeper knowledge is required in terms of toxic gases because Complex Pyrolysis Model would be more adequate.

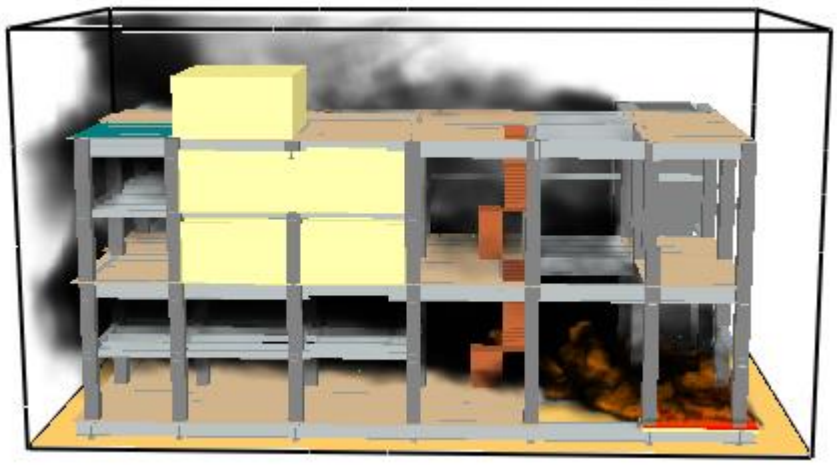

Figure 42. Smoke migration - Scenario 4B

6. REFERENCES

[1] Pula R., Khan F.I., Veitch B., Amyotte P., *Revised fire consequence models for offshore quantitative risk assessment*, J. Loss Prev Process Ind; 18: 443-54, 2005.

[2] Ufuah E., *Fundamental Behaviour of Offshore Platform Steel Deck Under Running Pool Fires*, School of Mechanical, Aerospace and Civil Engineering, Manchester, United Kingdom, 2012

[3] Bailey C., *One Stop Shop in Structural Fire Engineering*, University of Manchester

[4] Regulamento técnico de segurança contra incêndio em edifícios, Diário da República, 1.ª série, N.º 250, 29 de Dezembro de 2008

[5] Diário da República, 1.ª série, N.º 220, 12 de Novembro de 2008

[6] Stern-Gottfried J., Rein G., Torero J.L., Travel Guide, Fire Risk Management, November 2009, pp. 12-16

[7] PD 7974-1:2003, *Application of fire safety engineering principles to the design of buildings*. Initiation and development of fire within the enclosure of origin (Sub-system 1), BSI British Standards

[8] Zaharia R., *Lecture 1: Fire safety*, Lulea, 3 November 2014

[9] Pettersson O., Magnusson S-E., Thor J., *Fire Engineering Design of Steel Structures*, Publication 50, Swedish Institute of Steel Construction, 1976

[10] Eurocode 1: Actions on structures – Part 1-2: *General actions – Actions on structures exposed to fire*, European committee for standardization, November 2002

[11] McGrattan K., McDermott R., Weinschenk C., Hostikka S., Floyd J., Hughes J., Overholt K., *Fire Dynamics Simulator Technical Reference Guide Volume 3: Validation*, National Institute of Standards and Technology, Gaithersburg, Maryland, USA, and VTT Technical Research Centre of Finland, Espoo, Finland, 2015

[12] Wang L., Lim J., Quintiere J. G., *Validation of FDS predictions on fire-induced flow: a follow-up to previous study*, Fire and Evacuation Modeling Technical Conference 2011 Baltimore, Maryland, August 15-16, 2011

[13] Steckler K. D., Quintiere J. G., Rinkinen W. J., *Flow induced by fire in a compartment*, U.S. Department of Commerce, National Bureau of Standards, National Engineering Laboratory, Center for Fire Research, Washington, DC 20234, September 1982

[14] Zhang Ch., Li G., *Fire Dynamic Simulation on thermal actions in localized fires in large enclosure*, Advanced Steel Construction Vol. 8, No. 2, pp. 124-136, 2012

[15] Zhang Ch., Zhang Z., Li G., *Simple vs. sophisticated fire models to predict performance of SHS column in localized fire*, Journal of Constructional Steel Research, Volume 120, April 2016, Pages 62–69, 2015

[16] Rein G., Zhang X., Williams P., Hume B., Heise A., Jowsey A., Lane B., Torero J. L., *Multi-story Fire Analysis for High-Rise Buildings*, Edinburgh Research Archive, BRE Centre for Fire Safety Engineering, BRE Research Publications , 2007

[17] Sandström J., Cheng X., Veljkovic M., Wickström U., Heistermann T., *Travelling Fires for CFD*, Fire safety science, proceedings of the 10th international symposium, International Association for Fire Safety Science, London, 2011

[18] Stern-Gottfried J., Rein G., *Travelling fires for structural design–Part I: Literature review*, Fire Safety Journal, Volume 54, November 2012, p. 74–85

[19] Stern-Gottfried J., Rein G., *Travelling fires for structural design–Part II: Design methodology*, Fire Safety Journal, Volume 54, November 2012, p. 96–112 +3

[20] N. M. Petterson, *Assessing the Feasibility of Reducing the Grid Resolution in FDS Field Modelling*, Fire Engineering Research Report 2002/6, March 2002, University of Canterbury, Christchurch, New Zeland

[21] Kelsey A., Gant S., McNally K., Betteridge S., Hill H., *Application of global sensitivity analysis to FDS simulations of large LNG fire plumes*, Health and Safety Laboratory; Buxton, SK17 9JN; Shell Research Ltd, Shell Technology Centre Thornton, P.O. Box 1, Chester CH1 3SH, Symposium series no 159, 2015

[22] McGrattan K., Hostikka S., McDermott R., Floyd J., Weinschenk C., Overholt K., *Fire Dynamics SimulatorUser's Guide*, NIST Special Publication 1019 Sixth Edition, Baltimore, Maryland, USA, April 13, 2015

[23] Cheng X., Zhou Y., Yang H., Li K., *Numerical Study on Temperature Distribution of Structural Components Exposed to Travelling Fire*, State Key Laboratory of Fire Science, University of Science and Technology of China, Hefei, Anhui 230027, China, 2014

[24] Eurocode 3: *Design of steel structures - Part 1-2: General rules*, European committee for standardization, December 2005

[25] Vassart O., Zhao B., Cajot L.G., Robert F., Meyer U., Frangi A., *Eurocodes: Background & Applications Structural Fire Design, Worked examples*, JRC Science and Policy Reports, 2014

[26] Drysdale D., *An Introduction to Fire Dynamics (2nd edition)*, University of Edinburgh, Scotland, United Kingdom, 1998

[27] Karlsson B., Quintiere J., *Enclosure Fire Dynamics*, CRC Press LLC, Boca Raton, Florida, United States, 2000

[28] Morgan J. Hurley, *SFPE Handbook of Fire Protection Engineering Fifth Edition*, Aon Fire Protection Engineering, Greenbelt, MD, USA, 2016

[29] Heskestad G., *Luminous Height of Turbulent Diffusion Flames*, Fire Safety Journal, 5, 2, pp. 103–108, 1983

[30] Fleury R., Spearpoint M., Fleischmann Ch., *Evaluation of thermal radiation models for fire spread between objects*, Fire and Evacuation Modeling Technical Conference 2011 Baltimore, Maryland, August 15-16, 2011

[31] Thomas P. H., *The Size of Flames from Natural Fires*, Ninth Symposium (International) on Combustion, Combustion Institute, Pittsburgh, pp. 844–859, 1962

[32] Beyler C. L., *Engineering Guide: Assessing Flame Radiation to External Targets from Pool Fires*, Bethesda, MD: Society of Fire Protection Engineers, 1999

[33] Mudan K. S., *Geometric View Factors for Thermal Radiation Hazard Assessment*, Fire Safety Journal, 12, 2, pp. 89–96, 1987

[34] LNG Safety Research Program, Report IS 3-1, American Gas Association, 1974

[35] McGrattan K. B., Baum H. R., Hamins A., *Thermal Radiation from Large Pool Fires* (NISTIR 6546), Fire Safety Engineering Division, November 2000

[36] *Safety Considerations in Siting Housing Projects*, Department of Housing and Urban Development, HUD Report 0050137, 1975

[37] *Environmental Criteria and Standards*, 24 CFR Part 51, Subpart C, paragraph 51.201

[38] Howell, J. R. (2008), *A catalog of radiation heat transfer configuration factors, 3rd edition*, Department of Mechanical Engineering, the University of Texas at Austin, Austin, Texas 78712-1063, Retrieved 26 March, 2009, from: www.me.utexas.edu/~howell/

[39] D. Stroup and A. Lindeman, *Verification and Validation of Selected Fire Models for Nuclear Power Plant Applications*, NUREG-1824, Supplement 1, United States Nuclear Regulatory Commission, Washington, DC, 2013. 37

[40] Davis, W.D., Notarianni, K.A. and McGrattan, K.B., *Comparison of Fire Model, Predictions with Experiments conducted in a Hanger with a 15 meter Ceiling*, NISTIR 5927, National Institute of Standards and Technology, Gaithersburg, Maryland, USA, 1996

[41] Babrauskas V., *Estimating Large Pool Fire Burning Rates*, Article in Fire Technology, January 1983

[42] Lois E., Swithenbank J., *Fire Hazards in Oil Tank Arrays in a Wind*, Seventh Symposium (International) on Combustion, The Combustion Institute, Pittsburgh, 1978, pp. 1087-1098

[43] Blinov V.I., Khudiakov G.N., *Diffusion Burning of Liquids*, U.S. Army Translation, NTIS No. AD296762 (1961)

[44] *Combustion and fuels. Liquid fuels*, Politechnika Wrocławska, www.wme.pwr.edu.pl

[45] Ferek R. J., Ross J. L., Hobbs P. V., *Airborne Sampling of smoke emissions from the controlled burn of 20 000 gallons of crude oil during open ocean conditions off Newfoundland*, Final Report from University of Washington to State of Alaska Department of Environmental Conservation, March 1995

[46] M. Fingas, *Soot Production From In-Situ Oil Fires*, Spill Science, Edmonton, Alberta, Canada, 2011

[47] Overholt K., *Fire Plumes and Flame Heights*, Fire Dynamics ENGR 4420, -nie znalazłam jeszcze

[48] Overholt K., *Fire Dynamics – Heat Fluxes in FDS*, 26 January 2014, www.koverholt.com/2014/01/heat-fluxes-in-fds/

[49] Beyler, C. L., *Engineering Guide: Assessing Flame Radiation to External Targets from Pool Fires*, Bethesda, MD: Society of Fire Protection Engineers, 1999

APPENDIX A

EFFECT OF THE GRID RESOLUTION ON THE FLAME SHAPE

Scenario 4A, Mesh 20/40 cm

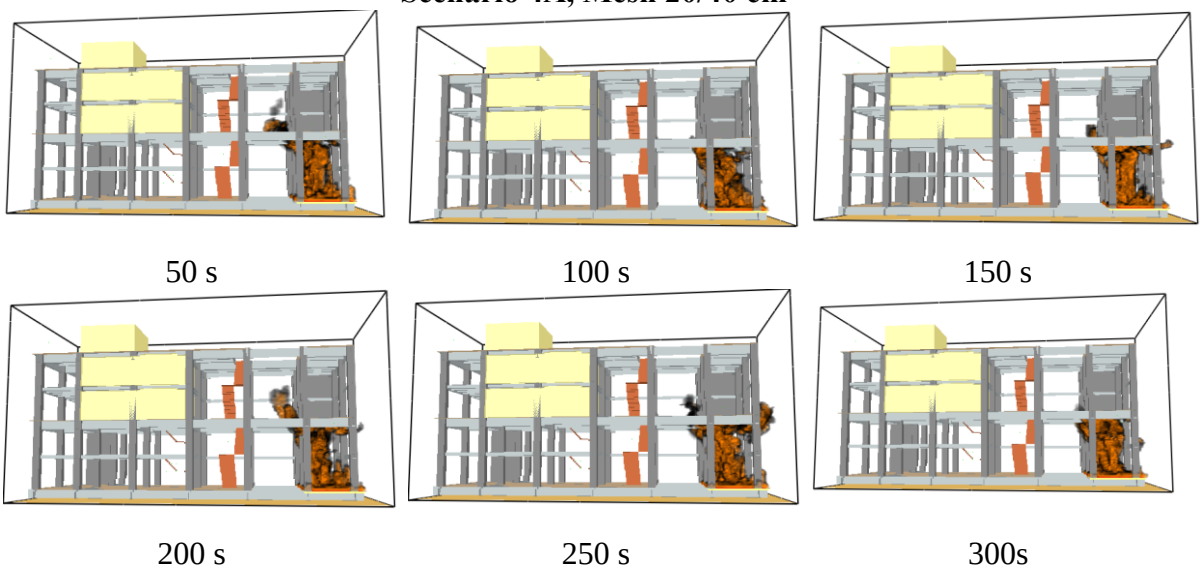

50 s | 100 s | 150 s

200 s | 250 s | 300s

Scenario 4A, Mesh 40 cm

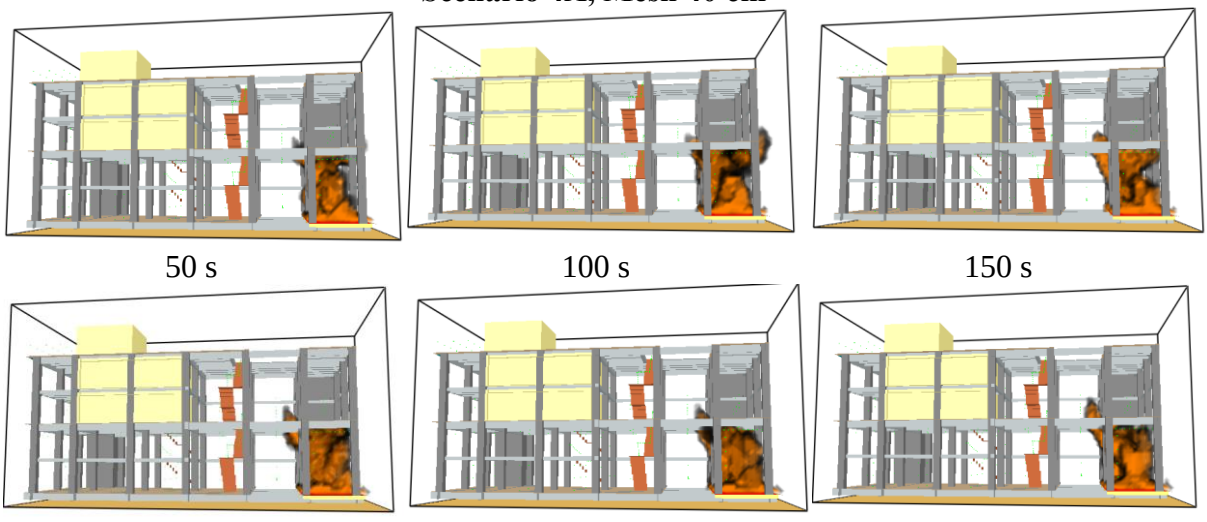

50 s | 100 s | 150 s

Scenario 4A, Mesh 80 cm

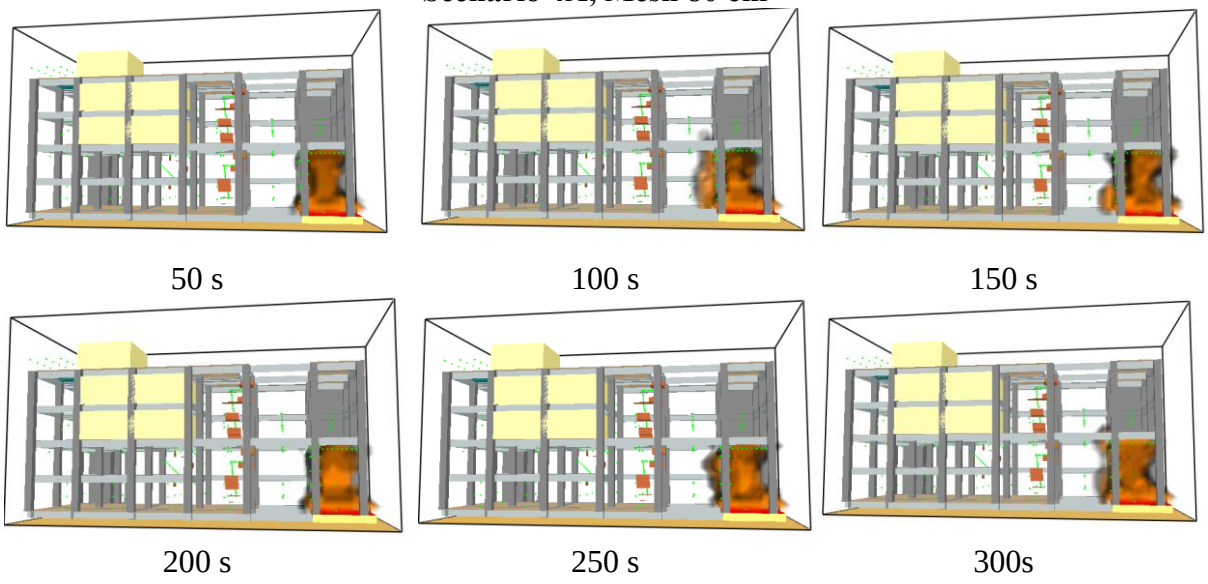

50 s | 100 s | 150 s

200 s | 250 s | 300s

Scenario 4A, Mesh 120 cm

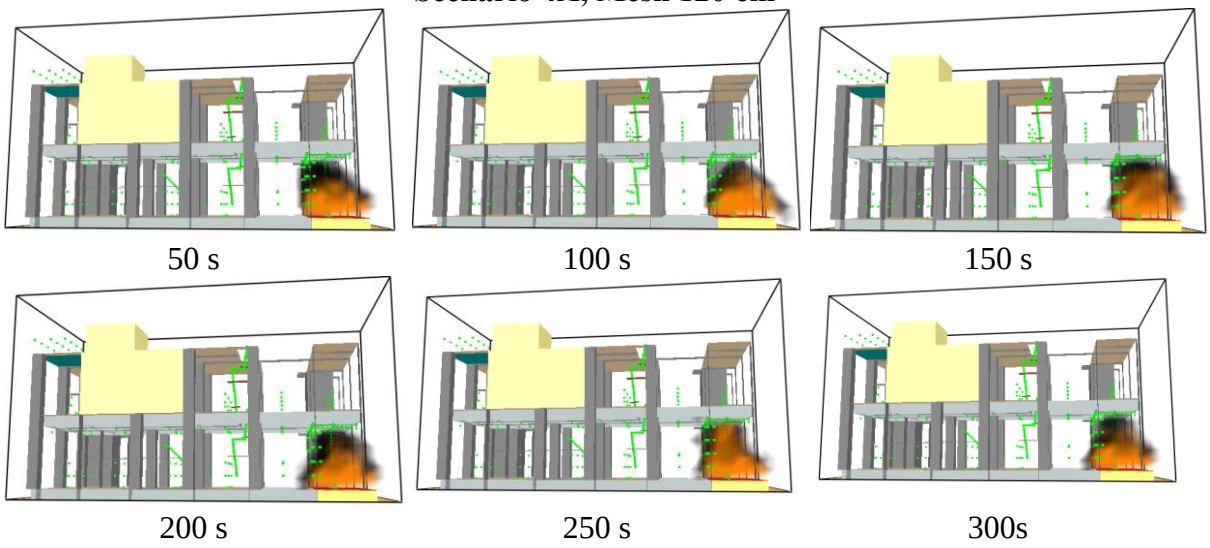

50 s | 100 s | 150 s

200 s | 250 s | 300s